Aalto-yliopisto
Aalto-universitetet
Aalto University

Master's Programme in Building Technology

Coupling the fire simulation and structural analysis through adiabatic surface temperature

Muhammad Humza Khan

Master's Thesis
July 11, 2022

Aalto-yliopisto
Aalto-universitetet
Aalto University

Author Muhammad Humza Khan

Title of thesis Coupling the fire simulation and structural analysis through adiabatic surface temperature

Programme Master´s in Building Technology

Thesis supervisor Prof. Simo Hostikka

Thesis advisor(s) Dr Octavian Lalu

Date 11.07.2022 **Number of pages** 74 + 6 **Language** English

Abstract

This study presents the results of one-way coupling between a fire simulation performed in computational fluid dynamics (CFD) and the structural response in finite element (FE) analysis. A built-in tool of adiabatic surface temperature (AST) in Fire Dynamics Simulator (FDS) is utilized for transferring the boundary conditions into SAFIR, a Finite Element package. A validation study is done using the experimental data where an unprotected steel column is subjected to a localized fire. The results from FDS-SAFIR coupling indicate good agreement with the experimental data however, some discrepancies at different time intervals are noticed. The thermal response is checked based on steel temperatures on all faces of column while the structural response in terms of horizontal and vertical deflections. A sensitivity analysis highlights that the material properties of steel and convective coefficients assumed have influence on both thermal and structural response. A comparison between AST surface and AST gas device indicates that a structure in a close proximity to fire has influence on the development of temperature and therefore it should be modelled as an obstruction in fire analysis. The coupling methodology is then used to investigate the forces redistribution and progressive collapse mechanism in a planar steel frame subjected to a localized fire. It is observed that the fire-induced stresses in a member are redistributed to the adjacent members, and this redistribution of forces continue even during the cooling phase. A comparison of different fire locations in the frame has highlighted that a fire on the central ground floor column and first-floor column is more detrimental to the overall stability of the structure. The analysis shows that a progressive collapse occurs due to a variety of phenomena like high load ratio, cantilever beam and pull-in force mechanism. Further investigation highlights that the addition of one bay to the frame does not significantly improve the forces redistribution however, increasing the stiffness of ground floor columns does improve the overall stability and performance.

Keywords CFD-FEM Integration, Adiabatic Surface Temperature, FDS-SAFIR one-way coupling, Progressive collapse mechanism.

Contents

Preface

This research study could not have been done without the support of several individuals, and to all of them, I would like to express my gratitude. The study is done remotely while working with my current employer, BRE (Building Research Establishment) in the UK. The support from Aalto university and BRE have proved to be very helpful in compiling the data and writing this thesis.

I would like to express my sincere gratitude to my academic supervisor Prof Simo Hostikka for his trust in me and a keen interest in the research topic. His efforts in formulating the proposal, defining the framework and valuable guidance at every step helped me a lot in completing this study. The enormous support from the PhD students working with Prof. Simo was invaluable for the completion of this work. Rahul Kallada Janardhan and Saani Shakil shared fire and structural analysis results from their research, which acted as a guideline for defining this study. The experimental data used in this study was shared by Dr Chao with Rahul and I am grateful to both for sharing it with me. Most specifically, I would like to express my gratitude to my industrial advisor Dr Octavian Lalu who helped me in understanding key concepts related to fire safety and advanced numerical analysis. For daily problems in structural modelling and analysis, industrial advisor was the first source of consultation.

On a personal note, I would also thank my manager Tom Lennon, principal fire consultant at BRE, for his approval and support in this thesis. His valuable suggestions and experience proved to be very effective in understanding the work. Finally, and not least important, I would like to thank my parents, family and friends for their wishes and support.

11 July 2022

Muhammad Humza Khan

Symbols and abbreviations

Symbols

$\boldsymbol{\varepsilon}$	Surface Emissivity
$\boldsymbol{h_c}$	Convective coefficient [W/m^2K]
$\boldsymbol{T_r}$	Temperature due to radiation [°C]
$\boldsymbol{T_g}$	Temperature due to convection [°C]
$\boldsymbol{\sigma}$	Stephan-Boltzmann constant [5.67x10$^{-8}Wm^2K^{-4}$]
$\boldsymbol{F_i}$	Configuration Factor

Operators

$\frac{\partial}{\partial x}$	Partial derivative in x
$\frac{\partial T}{\partial t}$	Partial derivative of temperature with respect to time.

Abbreviations

AST	Adiabatic Surface Temperature
FDS	Fire Dynamics Simulator
CFD	Computational Fluid Dynamics
BRE	Building Research Establishment
NIST	National Institute of Standards and Technology
FEA	Finite Element Analysis
FDM	Finite Difference Method

List of Figures

List of Tables

1 Introduction

The fire resistance rating of the supporting elements in a structure define the overall fire safety of a building. Prescriptive codes (AISC, EC) are followed in many countries which assume uniform heat exposure to the structural elements in a compartment. These design standards are based on the standard fire exposure which may not reflect real fire scenarios in any compartment. A standard fire test assumes a worst-case scenario in a fire situation where heating and cooling phases are neglected. It assumes uniform compartment temperature whereas the gas temperature distribution is highly non-uniform in localized fires [1]. A real fire in a compartment consists of three phases: a growth phase, flashover and fully developed fire [2]. A schematic of real and standard fire curve is illustrated in the **Figure 1**. Therefore, any design of a structure based on a standard fire resistance test may not represent the real fire safety level of a building. This argument can be supported by the observations made at full-scale fire tests conducted at Cardington [3].

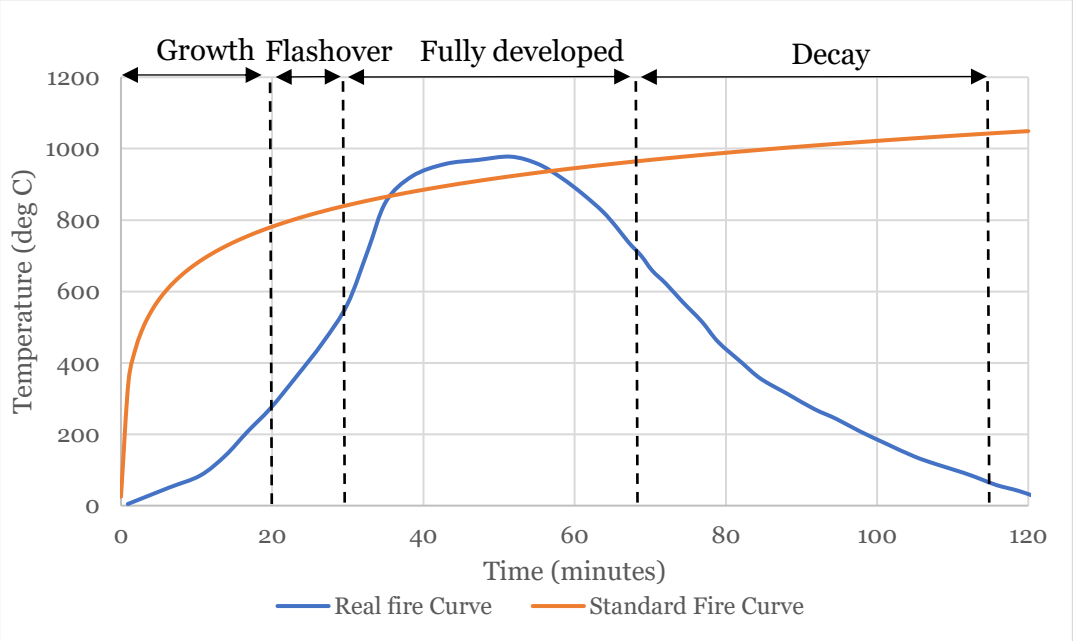

Figure 1: A schematic of difference between a standard fire and a real fire curve

In a fire compartment, additional forces are developed on structural members due to spatial and temporal variations of temperatures. These stresses and strains reduce the load-bearing capacity of a structure and will eventually lead to an accelerated failure [4]. The impact of fire loads on the steel members are detrimental, as [5] highlights that it is due to the loss of material strength and rigidity of steel at elevated temperatures. As compared to the other building materials like masonry and concrete, the fire safety level of a bare steel section is significantly lower. This is due to its material properties

i.e., high conductivity and low heat capacity. Therefore, the failure of structural steel is characterized by the time it achieves critical temperature. The critical temperature is classified as the temperature at which failure is expected to occur in a structural steel element for uniform temperature distribution [6]. The national annexe of Eurocode (BSEN1993-1-2) gives default values for critical temperature as a function of the utilization factor for steel. Most of the conventional structural design methods are based on these critical temperatures provided.

The performance of a structural member in a real fire scenario is also influenced by its surrounding members and the presence of restraint conditions. These factors have significant impact on the redistribution of forces and the failure of some members may lead to the progressive collapse in a frame. Progressive collapse mechanism is defined as a phenomenon where an initial local damage to a structural member spread to adjacent elements and eventually results in the collapse of whole structure. A study has highlighted that collapse of whole structure may be disproportionate to the original cause [7] which could be earthquake, fire or impact loading. In case of fire and thermal attack on one structural member, additional forces developed in a member may significantly exceed the load carrying capacity at ambient conditions. An example of such failure is the collapse of World Trade center where failure of several structural members resulted in the progressive collapse of the whole building.

This research study is focusing on the fire-structure analysis using CFD to FE one-way coupling approach as described in the literature. A validation study is done to compare the results from such coupling with an experimental data of a localized fire. Later, a case study is defined to investigate the forces redistribution mechanism and progressive collapse of a planar steel frame when one column is heated.

2 Literature review

2.1 CFD-FEM Coupling

Performance-based design is popular among structural fire engineers because of its more realistic approach toward a fire scenario. State of the art technologies like computational fluid dynamics (CFD) and finite element techniques allow designers to meet performance objectives without compromising the safety levels. Performance-based design methods provide greater flexibility in analysing each building component separately and adapt performance-based methods contrary to prescriptive rules [8]. One such approach for the analysis of fire exposed structures is CFD-FE coupling where the boundary conditions from Computational Fluid Dynamics are transferred into a Finite Element Analysis software. This methodology predicts an accurate response of structural components in a fire scenario. This form of integration between CFD and FEA is also known as the CFD-FEM integration approach. Conceptually, an interaction between fire development and the thermal response of a structure should be two-way. It means that the temperature variation in a compartment influences the thermal response of a structural element. Similarly, the thermal or structural response of a member influences the temperature development in the compartment. For example, as mentioned by [9], a deflection of a roof and a compartment failure might potentially modify the flow of the hot gases and smoke. The two-way coupling between two software is complex to achieve. The first challenge is finding an exact solution of several uncertainties present in such problem types. As it is understood that many physical phenomena associated with fire evolution do not follow deterministic rules [10]. For example, concrete spalling, heat leakages through cracks and internal pore pressures. The second reason for the complexity is the translation of boundary conditions from CFD into FEA software and vice versa which is not robust because the exchange of data may vary with the selection of two software. Two-way coupling has been performed previously in[10], [11]. However, prominent researchers in this field argue that such kind of coupling between fire models and structural response models have not yet yielded a satisfactory solution [12].

A simpler one-way coupling approach has also been implemented in various research publications[13–17]. This one-way coupling is also classified as a weak coupling approach as it does not involve the influence of a structural response on the fire development in a compartment [18]. In this approach, only the temperature development in a fire compartment has influence on the thermal or structural response of a member. From the CFD package, the gas temperature or heat flux varying in time and space, are imported as boundary conditions into an FEM package which then calculates the temperature distribution and structural response. Since the response of structure on fire development is not being studied in this approach, [11] claims that it may

optionally be omitted from the fire models in CFD analysis. However, others have emphasized that if the structure is engulfed in the fire flame and is impacting the fire then it should be modelled in the CFD [19]. Deep structural beams and large columns may interfere with the fire development in a way that their interference may affect the smoke flow path and formation of hot smoke reservoirs. One way coupling is further classified into FDS-FEM Interface method and FDS-FEM AST method. The coupling approaches described above between CFD, and FEM are illustrated below:

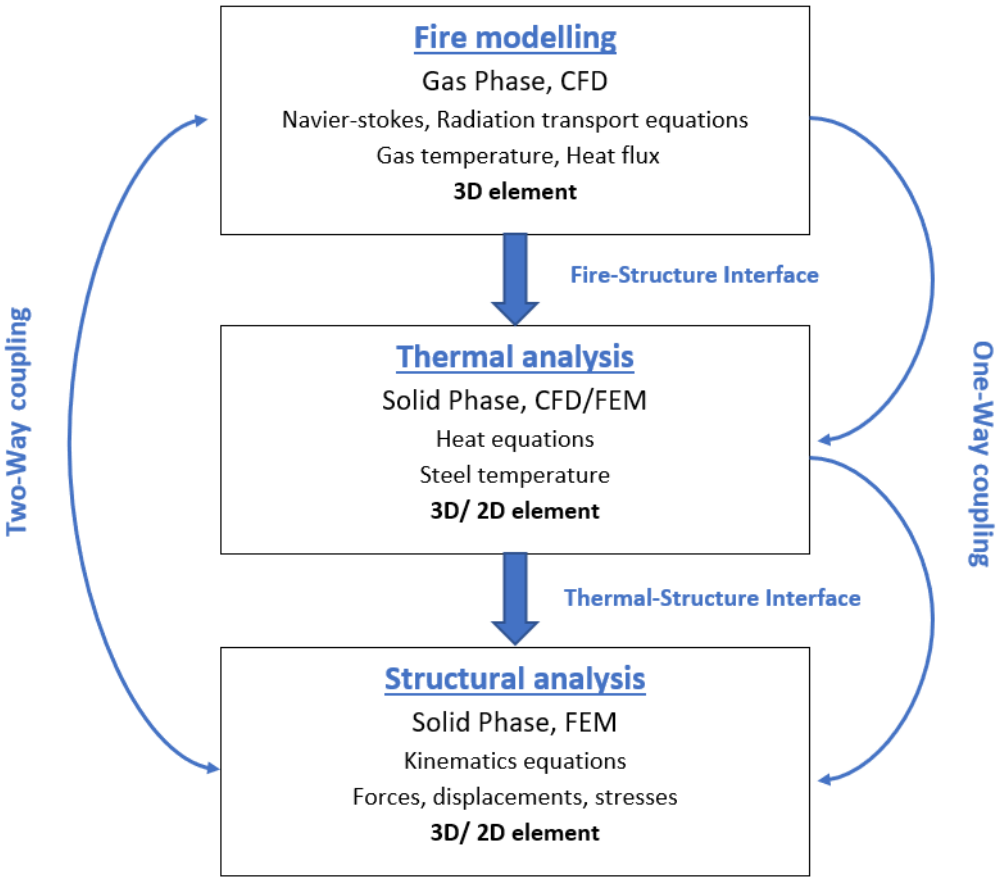

Figure 2: CFD-FEM coupling approaches for structural fire analysis[11]

Figure 2 is inspired by the study [11]. For CFD-FEM integration, the first step is to carry out the fire modelling where the geometry and simulation parameters are set up in a computational fluid dynamics software. The CFD runs the simulation and outputs the parameters like gas temperature, heat fluxes and radiation etc. The next step is importing the outputs of fire models which as boundary conditions into a finite element analysis software. A few CFD software can solve 1-D conduction problems by themselves however for 2-D and 3-D thermal analysis, using a finite element analysis software is the universal approach. The last step is of performing structural analysis which is done entirely in finite element analysis software. In one-way coupling, the

fire development is independent of the structure under investigation however, in the two-way coupling approach, the structural response predicts the future development of fire in the CFD simulation.

Both coupling approaches are found extensively in the literature however, currently there is no single CFD or FEM software that is capable of transferring the boundary conditions automatically. The reason is that most of the FEA software are not open source [18]. Another important reason, as reported by [20], is that the FDS domain is discretized into orthogonal cells in a rectilinear grid. However, SAFIR or similar packages take solid and shell elements. Therefore, the models in two packages do not match in coordinates and meshing criteria. FDS-FEM Interface method was originally developed for coupling FDS and SAFIR [21] however as reported in the case 2 validation study of [22], this method underestimates the temperature as compared to FDS-FEM AST method. Adiabatic surface temperature concept is developed in FDS as an inbuilt device known as AST which can measure the incoming heat flux on a surface by assuming it as a perfect insulator. The total incident energy is a combination of convective and radiative heat flux. The only condition for AST device approach, as reported in [23], is that the AST node must not be contained within a solid material. This means that defining an AST device inside a hollow section will not capture accurate temperature development. The detailed reason for this lies in the definition of an AST device itself which is explained in the section 2.1.1.

The first part of this research study is on the validation of Adiabatic Surface Temperature developed by Wickström. The data reported by an experimental program is compared to the results obtained through FDS-SAFIR one way coupling. Such kind of validation has been done previously in the literature using other software however, due to more flexibility and popularity of SAFIR among fire engineers, the procedure is repeated in SAFIR to observe any differences. As described earlier that some researchers have pointed out that if the structural member is influencing the fire development and the flow path of residual gases then it should be modelled in the CFD otherwise not. This argument is validated in this research study by modelling the obstruction in the CFD package and then comparing the results with the simulation without such obstructions. Finally, the structural response of the component is compared with the experimental observations and the differences in the results of SAFIR are reported.

2.1.1 Adiabatic Surface Temperature

The concept of Adiabatic Surface Temperature was introduced by Wickström[24] for transferring the thermal boundary conditions from the CFD package into FEA software. The idea to develop this concept was to extract one quantity from a CFD package which can then be transferred into finite element software instead of extracting heat flux, surface temperature and convective coefficient separately. An AST, in theory, is a fluid phase temperature at the face of a structural component under investigation. The structure of the surface where AST is calculated is considered as an Adiabatic surface in CFD simulation. Any adiabatic surface means that there is no heat transfer from or to the surface. The total heat flux to an ideal surface of a perfect insulator is by definition zero [25]. In simple words, Adiabatic surface temperature acts as a plate thermocouple installed on the face of a surface under investigation.

Wickström considers that the surface is perfectly insulated with the boundary conditions of a real surface. The fluid temperature adjacent to this insulated surface is captured. The adiabatic surface temperature was developed with the following two assumptions:

- The emissivity of soot is unity.
- The configuration factor is one.

Both assumptions may not be always true or universally applicable. The first assumption of unit emissivity of soot is rarely observed in a fire scenario. It is assumed that the soot density is uniform in a fire compartment. In simple words, the smoke is completely enveloping a structural member under investigation. However, we know from the zone modelling that a fire compartment has two zones. A hot upper layer and a cold bottom layer. At the lower part, due to an optically thin environment, the radiation and convective gas temperature might not be calculated very accurately in the AST outputs. This is applicable at the lower part of a structural column. Similarly, at the upper part of the compartment, where the soot and smoke density is higher, the time temperature might be poorly averaged. [18] claims that the results may not be accurate in the real fire scenario where the soot is not distributed uniformly. Similarly, in the case of travelling fires, where the fire area is large and highly non-uniform, it is not possible to have a unit emissivity of gas at the far-field region.

The second assumption of the unit configuration factor means that a surface under investigation is receiving radiations from all the sources in a compartment. It is true if the surface of a structural component is facing the fire source however, in the case of a concave surface, the configuration factor will be lower than one. The adiabatic surface temperature is a combination of temperature developed by radiation and the fluid flow over a surface. Joakim Sandström graphically illustrated this concept [26] in his thesis. It states that

the temperature of any adiabatic surface depends on the relation between ε and h_c and assume a value between T_r *and* T_g. Here, ε is the surface emissivity, h_c is the convective coefficient of the fluid, T_r is the temperature due to radiation and T_g is the temperature due to gas.

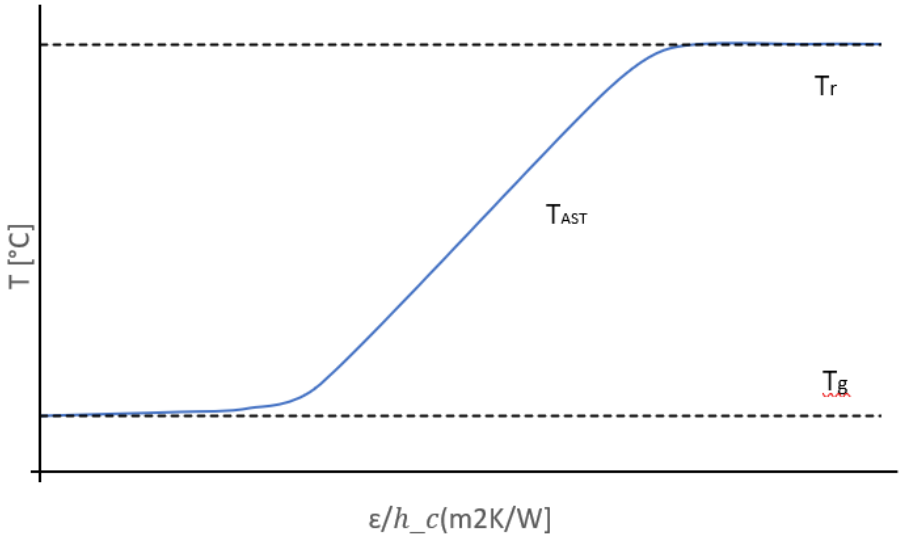

Figure 3: AST intervals between Tr and Tg [26].

Regardless of the assumptions made in the development of the AST concept, it is a robust practical approach for transferring CFD data into FEA software. It extracts one quantity in terms of temperature which is easily imported into a finite element software. This single quantity is based on two quantities which are temperature due to radiation and temperature due to gas flow. Several validation studies have been done for CFD-FEM coupling using the AST approach and the results have been reported very close to the experimental observations[18], [23], [24]. One study[27] on such coupling using AST reported the measured heat flux within 6% and overprediction of the steel temperature within 11% variations. It shows that this approach predicts close to realistic results.

Heat transfer phenomena between a burning fuel source and the surface under investigation are captured by AST. The analytical way of getting AST is described below in the form of mathematical equations. As we know that the total incoming heat flux is the summation of radiative and convective heat fluxes.

$$\dot{Q}_{total} = \dot{Q}_{radiation} + \dot{Q}_{convection} \quad (1)$$

The effective radiation flux on a surface is the difference between any incoming radiations and the radiations being emitted from the surface.

$$\dot{Q}_{radiation} = \varepsilon\left(\dot{Q}_{incident} - \sigma T_{surface}^4\right) \quad (2)$$

Here, ε is the emissivity of all the sources in a compartment and σ is the Stefan-Boltzmann constant. As we know that the incident radiation flux is the summation of all the fluxes from all directions in a compartment fire. It is written as:

$$\dot{Q}_{incident} = \Sigma_i \varepsilon_i F_i \sigma T_{source}^4 \quad (3)$$

Here, Σ_i denotes summation of all the terms. F_i is the configuration factor which is also known as the view factor. Since in adiabatic surface temperature, Wickström has assumed that the emissivity and configuration factor is considered as unity. Therefore, the above equation can be re-written as:

$$\dot{Q}_{incident} = \sigma T_{radiation}^4 \quad (4)$$

Here, $T_{radiation}$ is the temperature of the source emitting radiations. Now eq. 2 can be re-written as:

$$\dot{Q}_{radiative} = \sigma\left(T_{radiation}^4 - T_{surface}^4\right) \quad (5)$$

The convection heat flux can be expanded as:

$$\dot{Q}_{convective} = h_c\left(T_{gas} - T_{surface}\right) \quad (6)$$

Incorporating the above two equations into equation 1.

$$\dot{Q}_{total} = \sigma\left(T_{radiation}^4 - T_{surface}^4\right) + h_c\left(T_{gas} - T_{surface}\right) \quad (7)$$

Here, as we have assumed that an adiabatic surface is a perfect insulator that is there will be no heat transfer to or from the surface. The emissivity and heat transfer coefficients of an adiabatic surface are same as a real surface. Therefore, $T_{adiabatic}$ is the temperature of surface which is written as T_{AST} and the above equation is written as:

$$\dot{Q}_{total} = \sigma(T_{radiation}^4 - T_{AST}^4) + h_c\left(T_{gas} - T_{AST}\right) \quad (8)$$

The T_{AST} is calculated in FDS using an inbuilt tool therefore, the above equation is left with,

$$\dot{Q}_{total} = \sigma(T_{radiation}^4) + h_c\left(T_{gas}\right) \quad (9)$$

This is how an adiabatic surface temperature calculates the incoming energy due to only radiation and convection and transform it into one quantity.

2.1.2 Fire Dynamics Simulator

For an accurate representations of enclosure fires in terms of fluid chemistry and fire development, Computational Fluid Dynamics (CFD) simulations are often used. Several computational fluid dynamics software is available in the market like SOFIE, JASMINE, FDS, VESTA etc. In complex fire scenarios, Computational Fluid Dynamics (CFD) is considered to be more robust and accurate in terms of fluid chemistry. One of the most widely used CFD packages for fire simulations is FDS (Fire Dynamics Simulator). Fire Dynamics simulator is a large-Eddy simulation-based CFD package developed by NIST [28]. The package was first released in early 2000 for public use and has been through a continuous verification, development, and validation process. It is one of the most widely used software in the fire safety industry due to its robust approach in capturing fire and fluid evolution. The FDS package is capable of exporting the fluid temperature on a surface by incorporating the Adiabatic Surface Temperature (AST) concept defined as a device. As explained earlier, the adiabatic surface temperature approach was developed by Professor Ulf Wickström [24] for expressing the thermal exposure to a solid surface. FDS outputs this temperature in the form of a file which can then be used in any Finite Element Analysis software.

Discretization calculations of mass, energy and momentum done in FDS is by Finite Difference Method, FDM [29]. The net heat flux is calculated as described in the equation below:

$$\dot{Q}_{radiation} = \epsilon_s\left(Q_{incident} - \sigma T_{surface}^4\right) \tag{10}$$

To predict the next value at a certain time-step, the Taylor series is chosen as a continuous function. The Taylor series written in the general form is described as:

$$f(x) = f(a) + \frac{f'(a)}{1!}(x-a) + \frac{f''(a)}{2!}(x-a)^2 + \frac{f'''(a)}{3!}(x-a)^3 + \cdots \tag{11}$$

In FDS, the first-order Taylor series is applied to solve the radiative heat flux equation implicitly. Here, a is assumed as T^n and x is considered as T^{n+1}, n = number of time steps. The above equation now becomes,

$$T^{(n+1)^4} = T^{n^4} + 4T^{n^3}(T^{n+1} - T^n) \tag{12}$$

Graphical representation of the next value in the series is shown as:

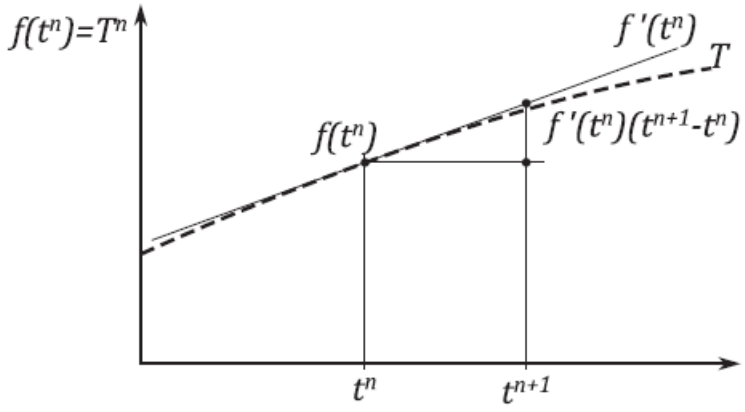

Figure 4: Taylor series in FDS

Combining the above two equations give:

$$Q_{radiation}^{(n+1)} = \epsilon\sigma\left(\frac{Q_{incident}^{(n)}}{\sigma} + 3T_{surface}^{n^4} - 4T_{surface}^{n^3}T_{surface}^{(n+1)}\right) \tag{13}$$

As we know that the total heat flux due to convection is given by:

$$Q_{convection}^{\cdot} = h_c(T_g - T_s) \tag{14}$$

FDS implicitly calculates the convective heat flux just like radiation equations in the Taylor series. It is written in the form,

$$Q_{convection}^{(n+1)} = h_c\left[T_g^n - \frac{1}{2}\left(T_{surface}^n + T_{surface}^{(n+1)}\right)\right] \tag{15}$$

h_c is the convective heat transfer coefficient and it depends on the Reynold number and Prandtl number of the fluid under observation. Therefore, it can be written in the form,

$$h_c = \max\left[\mathrm{C}(T_g^n - T_{surface}^n); \frac{k_{air}}{L}0.0037Re^{4/5}Pr^{1/3}\right] \tag{16}$$

The general form of heat balance equation at any surface is written as:

$$Q_{total}^{(n+1)} = Q_{radiation}^{(n+1)} + Q_{convection}^{(n+1)} \tag{17}$$

The above equations are written by understanding the calculation procedures presented in [30].

2.1.3 SAFIR

Thermal and structural response of an element has been studied in various Finite Element software like ABAQUS, SAFIR, ANSYS and LS-DYNA etc. A comparative study[31] has found that three software (ABAQUS, ANSYS, SAFIR) give close results for 3-D structural analysis. In ABAQUS there is a possibility of two-way integration, however, In SAFIR, integration is done by using either Adiabatic Surface Temperature (AST)[24] or the FDS-FEM interface method [32]. Both are weak-coupling approaches (i.e., one way). One study[19] has found the FDS-FEM AST methodology to be more accurate in case of localized fires. SAFIR is widely used finite element software in the fields of structural fire engineering. This software package allows the modelling of structures in fires by taking into account the complex material and geometrical non-linearities. As reported by [21], thermal elongation as well as a reduction in strength and stiffness of the materials at elevated temperatures is also taken into account. It is relatively simpler than other finite element software and is enriched with the library of elements and materials. Several validation studies have been done in SAFIR in the past [33–35] and has found results very accurate to the experimental observations.

SAFIR is capable of performing 2-D as well as 3-D thermal and structural analysis. The underlying concept for the development of SAFIR is that almost all structural elements are made up of solids therefore, only conduction is the mean of heat transfer. SAFIR also incorporates heat transfer by convection and radiation in the voids of structural elements. For example, the cavities present in the interior of hollow steel sections. As described in the technical reference guide of the software, the gas in the cavity is considered transparent to the radiation and has no specific heat [36]. For conduction in the solids, heat exchange is based on the Fourier series equations. The equation is represented as:

$$\frac{\partial}{\partial x}\left(k\frac{\partial T}{\partial x}\right)+\frac{\partial}{\partial y}\left(k\frac{\partial T}{\partial y}\right)+\frac{\partial}{\partial z}\left(k\frac{\partial T}{\partial z}\right)+Q=c\rho\frac{\partial T}{\partial t} \tag{18}$$

Here, {x,y,z} are the vector of cartesian coordinates. T is the temperature in Kelvins, k is the thermal conductivity in W/mK, Q is the heat generated within the system in W/m^3, ρ is the specific mass in Kg/m^3, c is the specific heat in J/KgK, and t is the time in seconds.

2.2 Progressive Collapse Mechanism

Several studies have been carried out in the literature to investigate the progressive collapse of a structure and the redistribution of forces [37–41]. In case of fire, when a structural member is heated at high temperatures, internal forces start to develop due to the tendency of member to expand. These additional forces are redistributed to adjacent structural elements which are relatively cooler. Redistribution of forces in a structure generally leads to an improved performance however failure of some members may lead to the collapse of whole structure. A parametric study has investigated the progressive collapse phenomena when one column was heated [37]. Three main failure modes have been identified in such scenarios named as: high load ratio member failure, cantilever beam mechanism failure and pull-in force mechanism.

In high load ratio member failure, the forces developed during the fire exceed load carrying capacity of a member and it results in the failure. In cantilever beam mechanism, due to excessive deflections, upper half of the beam thickness is in tension while the lower half is in compression resulting in the crushing of fibers, eventually leading to the failure of the member. The pull-in force mechanism is more dominant when an inner column of a frame is heated. After buckling of the member due to fire, the adjacent beams act as catenary to redistribute the vertical loads. As reported by [37], the load redistribution increases the compressive forces in the adjacent columns at heated floor and below. This catenary action of beams induces lateral pull-in force, and the adjacent columns may fail resulting in the progressive collapse of the structure.

3 Research Objectives

Following research objectives are set for this study.

3.1 Validation in SAFIR

The results from the reported experimental data are compared with the results obtained through FDS-SAFIR one way coupling. The objective is to investigate how SAFIR predicts thermal response in a localized fire scenario. Temporal and spatial variation of temperature calculated in SAFIR are compared with the experimentally reported data. For all the inaccuracies in the results, a sensitivity analysis is done to find out the important factors influencing the results.

The structural response of the component under investigation is compared with the experimentally reported data. It is investigated how accurately SAFIR can predict the structural response in case of localized fires. Investigating the differences if any will help understand the factors influencing the results.

3.2 AST vs AST-gas approach

Many researchers have reported that if the structural component under investigation is influencing the fire development or is impacting the flow of gases then it should be modelled into a CFD package. However, if there is no such influence then AST devices can be used in the CFD package without modelling the structural member. This research study is comparing the results obtained from both approaches and any differences in temperatures are reported.

3.3 Progressive collapse mechanism

A parametric analysis is done to investigate the most vulnerable columns of the steel frame structure when subjected to localized fire. Various failure modes and redistribution of forces during a localized fire is studied. The objective of investigating the global collapse of the structure is met by investigating the distribution of forces during the heating and cooling phases of fire. The focus of study is the redistribution of axial forces in columns as they are critical member of a structure and failure of such members may result in the collapse of whole structure.

4 Methodology

4.1 Validation study

The methodology devised for this research study is inspired by a publication [42] where the experimentally reported data is compared with the results obtained from CFD-FEM coupling using two different approaches. The experimental data are taken from the publication presented at the Fourth International Workshop on Structures in Fire in Portugal. In this study, the mechanical response of a steel column is reported when exposed to a localized fire [43]. Fire resistance experiments were done on a square steel column when exposed to a localized fire. Four tests were conducted with various restrain conditions the mechanical response was observed. Case 1 is under investigation in this research study where the column is fixed at the base and has a free end at the top. The time-temperature data for this case is reported in the paper and therefore can easily be compared.

Several AST devices will be placed on the modelled surface of a column in the CFD package, and the output is exported in a separate file. This time-temperature file is then imported into the SAFIR and the thermo-mechanical response of the structure is investigated. The results obtained from the thermal analysis and the structural analysis are then compared to the experimentally reported data. The results are followed by a sensitivity analysis to find out the factors responsible for differences.

4.1.1 Experimental setup

A square steel column with hollow section is subjected to a localized fire and is under investigation. A load-bearing frame was used with an oil jack having a maximum output of 490KN. The specimen was set up just below this steel frame. The electric hydraulic pump was controlling the oil jack and this pump was operated from the outputs of displacement gauges and load cells through the digital indicator. A detailed description of the experimental arrangement is written in the publication [43]. The experimental arrangement is illustrated in **Figure 5**.

A 0.3m square propane diffusion burner was placed adjacent to the base of the column. The heat release rate of propane was set as 52.5 kW. The burner was placed at a height of 0.25m from the base of the column. A square steel column (STRK400, 0.1m x 0.1m, 3.2mm and 1.6m tall) was used. In case 1, the temperature at four faces of the column at various locations. Type-K (Chrome-alumel) thermocouples were used with a 0.65mm diameter bead. These thermocouples were fixed on the specimen surface with spot-welded steel foil. The location for temperature measurement is shown in **Figure 6** . In case 1, vertical and horizontal deformations were measured with displacement gauges. The schematic of case 1 is shown in **Figure** 7.

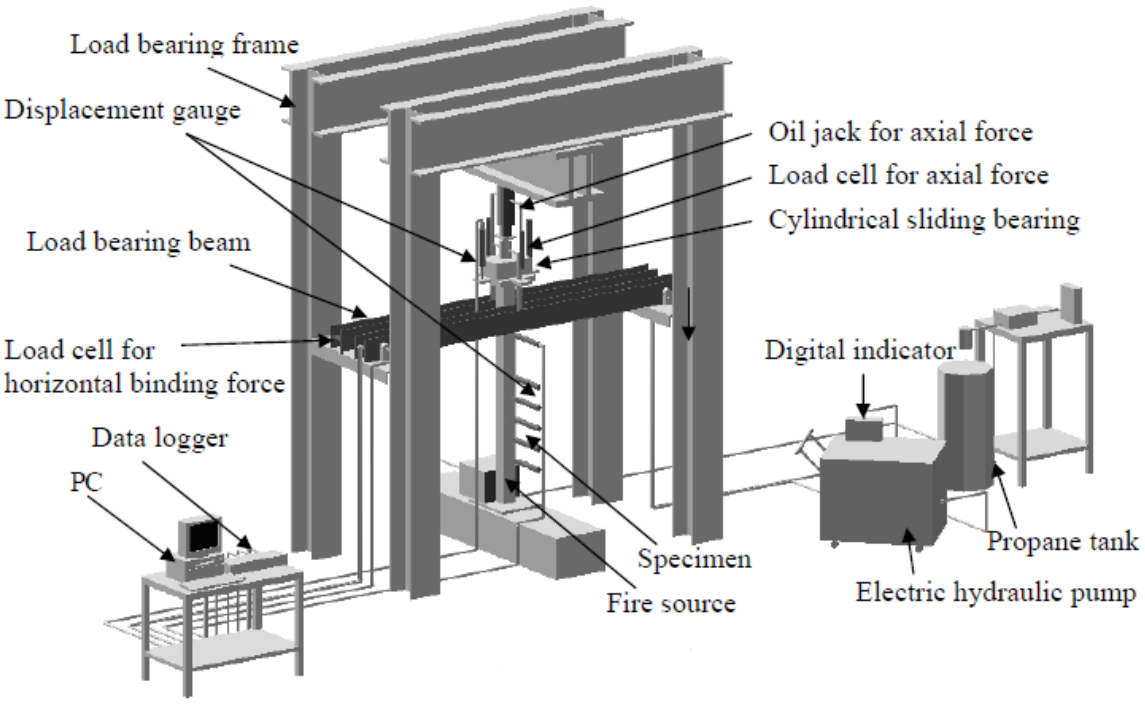

Figure 5: Test arrangement as reported by [43]

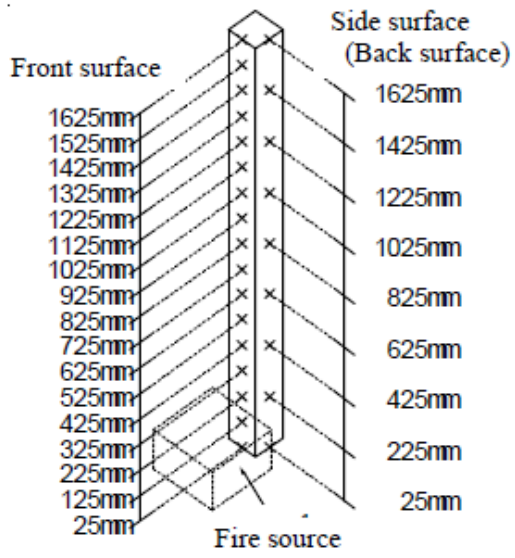

Figure 6: Location of type-K thermo-couples

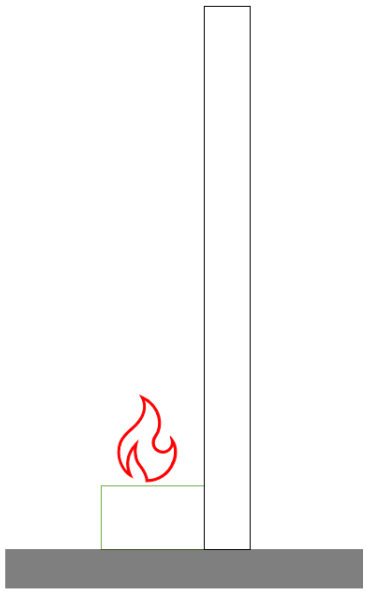

Figure 7: Schematic diagram of case 1

4.1.2 FDS Code

The experimental setup as described above is modelled in FDS. Two cases are built-in FDS, one where the steel column is created as an obstruction and the AST devices are placed on the face. In second, there is no column modelled in FDS and the AST devices are placed in the air. The temperature distribution is supposed to be different in both simulations. The influence of column obstruction on fire and the flow of combustion gases is investigated in this case.

FDS modelling and resulting data is provided by the academic advisor of this thesis project. The computational domain in FDS is set to 0.75m x 0.45m x 1.8m. The cell size in each mesh is 0.025m. Propane is defined as fuel and the same parameters are given for heat release rate and other geometrical features as described in the experimental setup. Adiabatic surface temperature devices are placed on each face of the column at a distance of 5cm over the height. The graphical representation of FDS modelling can be seen in the picture below which is captured from smoke view.

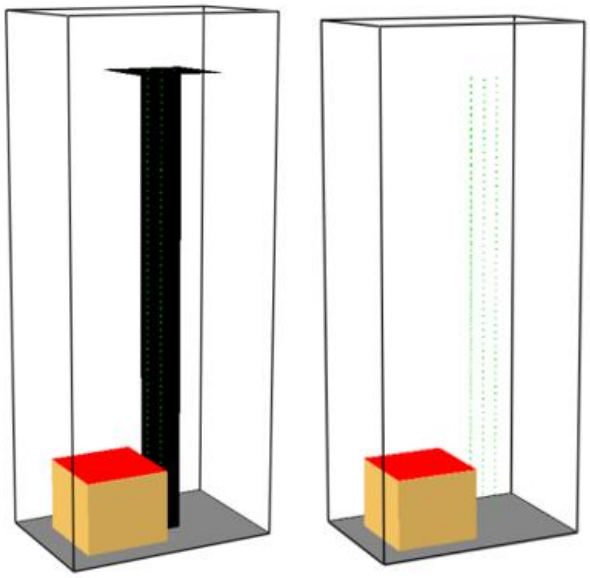

Figure 8: FDS models with and without steel columns as an obstruction.

The AST devices are set up on each face of the steel column. To get an accurate location of the device and the direction for capturing radiation and convective energy transfer, it is important to specify the orientation of the device. Each surface of the column was assigned a face orientation and AST devices were located on each face of the column. The location of a device is specified using XYZ coordinates in FDS and orientation is specified by IOR command. Following command is used for defining an AST device.

"&DEVC ID ='AST', XYZ='...', IOR='...', QUANTITY='ADIABATIC SURFACE TEMPERATURE'/"

For the FDS simulation without steel column modelled as an obstruction. The AST device is defined using following command line:

"&DEVC ID ='AST', XYZ='...', IOR='...', QUANTITY='ADIABATIC SURFACE TEMPERATURE GAS'/"

4.1.3 SAFIR models

Column geometry is constructed in SAFIR using 3D solid finite elements. Geometry is modelled in GID software[44] which is the pre-processor for SAFIR. The output of SAFIR is visualized in the post-processor software known as Diamond [45]. The geometry is created in the SAFIR problem type known as 'Thermal 3D'. The output from the thermal analysis will be used as an input for the subsequent structural analysis. The modelling is done as guided by the SAFIR solid 3D training module [46].

The base of the column is fixed, and the top is set free as reported by case 1 of the experimental setup. The cross-section is created in the Global x-y plane using lines and the height of the column is in the Global z-axis. The height of the column is divided into small sections to assign time-temperature data from AST file. The first section is set to 0.25m since the height of the burner is 0.25m from the base. There will be no direct heat transfer from the surface of burner to the bottom of the column. The only mode of heat transfer to the bottom is conduction within the steel. The next section is 50mm and all the sections above are 100mm. Each face of a section creates two surfaces in SAFIR. One outer surface and the one facing inwards. The AST files are assigned to the outer surface since the data captured from CFD is on the outer face of the column.

Boundary conditions

One AST file at a certain location is applied on the face of the column assuming that the temperature will be relatively uniform for each face of the section. It is difficult to divide the column into a large number of sections and apply the AST file at each. For instance, the AST file at z = 0.275m is applied to the surface having dimensions (z=0.25-0.3m). In this way, 14 AST files are applied on the front face, 14 on the left side, 14 on the right side and 14 on the backside. The geometry of the column and different AST files applied as frontier boundary conditions are illustrated in the figure below:

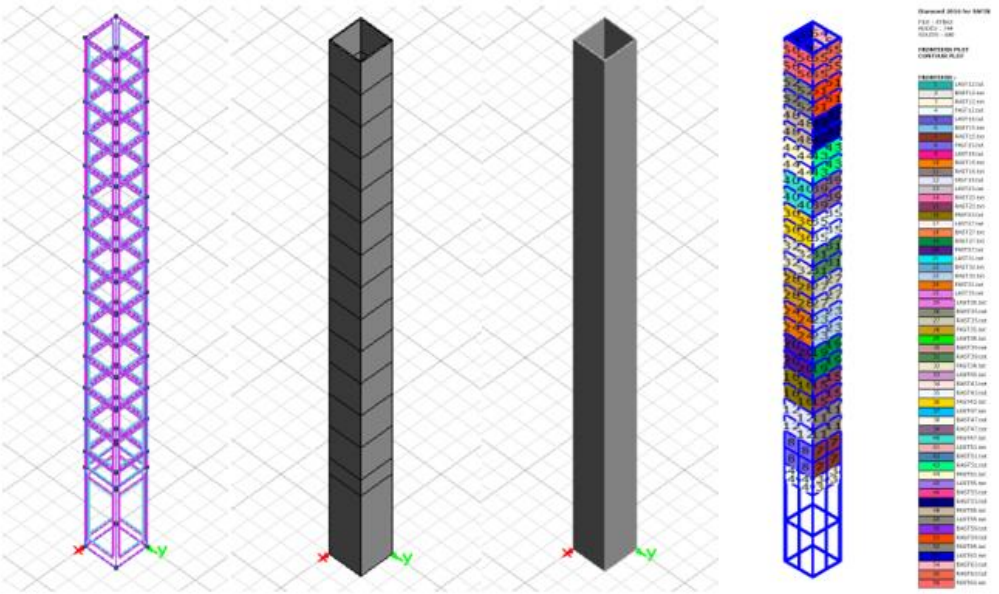

Figure 9: Column geometry in SAFIR, AST applied as frontier constraints.

Material properties

Material properties of the steel are assigned using the Eurocode[6]. Temperature-dependent values of thermal conductivity, specific heat and yield stress are taken from the Eurocode and assigned in the SAFIR modelling. Material properties used in the SAFIR analysis are presented in Appendix A. By default, value of convective coefficient hot is taken as 25 in SAFIR and convective coefficient cold as 4. Relative emissivity of steel is 0.7. Authors tried to change these parameters to find the variation in temperature distribution. The results are described in the sensitivity analysis section.

Problem data

Problem data is defined using a PARDISO solver and specifying the number of cores to 1. This solver is meant for assigning the extra number of cores on a computer however; as reported in the SAFIR manual on thermal calculations, using more than 1 core does not influence the time of calculation significantly [47]. The value of TETA is kept at 0.9. As described in the SAFIR manual, specifying the zero value runs the program in a nearly explicit manner. Specifying it as one will lead to fully implicit integration. 0.9 value has been used consistently by the developers and therefore has been adopted in this study. T_INITIAL is kept at 20 which means that the temperature at the start of simulation will be 20 °C. TIMESTEP is kept as 1. This function is used for the time integration of calculations and is measured in seconds. Smaller time steps will output accurate results. UPTIME is the total time of calculation and is kept as 7200 seconds since the experimental data reported by

Kamikawa was for 2 hours. TIME PRINT is also kept as 1 second to visualize the time-temperature distribution at each second in the post-processor.

Mesh is created by assigning the number of cells to all the volumes possessed by the steel columns. The current version of the GID license at Building Research Establishment (BRE, UK) supports only 1010 nodes for SAFIR modelling. Therefore, only 2 cells were assigned to each face of the column section (0.1m x 0.1m). It resulted in one square cell of 50mm and a total of 744 nodes with 480 solid surfaces created in the thermal model.

Structural modelling

Structural modelling was initially planned to be done after thermal analysis by updating the SAFIR problem type from 3D-thermal analysis to 3D-structural analysis. The structural model would use the same geometry, materials and meshing parameters as assigned in the thermal model. The output file from the thermal model was to be imported into the structural model and was planned to be assigned in the material section of GID. Loading and supporting conditions were replicated as in case 1 of the experimental setup. Therefore, the column was fixed at the base and free at the top end. For structural calculations, the calculation parameters were updated.

However, as is explained in section 0, SAFIR does not calculate the heat transfer through a cavity in a 3-D thermal model. Therefore, the structural modelling was done in a different way. A frame was defined in 3-D structural problem type with the height of 1.6m and was divided into 4 sections. Each section is assigned an output of 2-D thermal analysis in the form of a *TEM file. No loading was applied, and the base of the column was fixed while keeping the top free. An additional x-constraint was applied at 1392mm to replicate test case 1. Only 4 different 2-D sections are applied to effectively observe the response in the post-processor. Additional sections when applied make

the *XML file extremely large in size and makes the Diamond to run very slow to visualize the data.

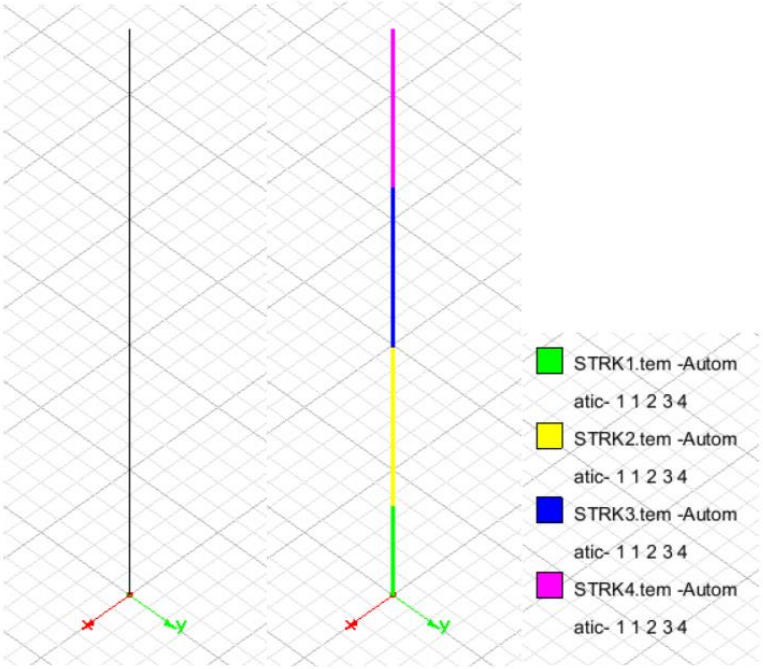

Figure 10: Column geometry in SAFIR problem type 3-D Structural

The STATIC PURE NR is chosen for loads since the analysis is being done at elevated temperatures. The convergence is chosen as COMEBACK with a TIMESTEPMIN of 1 second. According to the SAFIR structural manual, if no come back is chosen for convergence, the simulation will stop if the stiffness matrix is not positive definite. When a comeback is chosen, if the stiffness matrix is negative in a one-time step, the overall time for the simulation is reset to the last convergence point and the simulation start from the timestep divided by 2 [48]. PRECISION is the small tolerance value reached to have convergence. NGSHELLTHICK is the number of integrations on the thickness of the element, and it is kept at 3.

To find out the effect of number of divisions on steel column for SAFIR modelling, a second approach is applied where the column is divided into 15 sections. This is to find out if more divisions make the results accurate or not. Each section of column is assigned a 2-D thermal model whose thermal analysis was already done using relevant AST time-temperature curve. A total of 60 AST files are extracted from SAFIR at relevant heights as illustrated in the figure below.

Each 2-D thermal model is run including torsional analysis for subsequent structural modelling. A total of 15. *TEM files are exported in 3-D frame structure by assigning them as beam element properties. No loading is applied as in case 1 of the experimental scheme. Mass of column is kept as zero

and the structural modelling is done using STATIC PURE NR. The figure below presents the section used for second structural analysis.

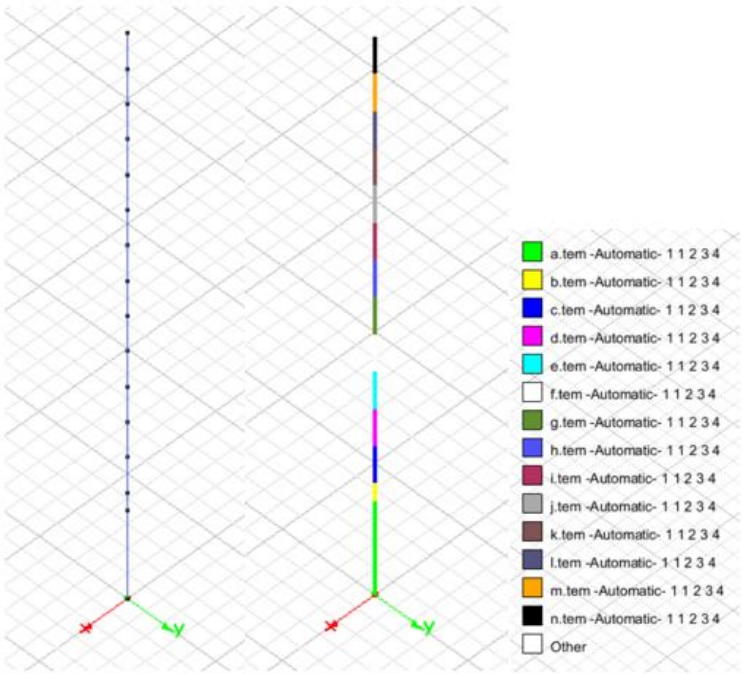

Figure 11: Applying 15 output files from 2-D thermal into 3-D SAFIR

4.2 Progressive collapse mechanism

To study the redistribution of forces and the progressive collapse mechanism in fire, a frame is considered which is subjected to a localized fire. To obtain a realistic time-temperature data for a localized fire, a simulation is carried out in FDS. The data obtained from FDS is then transferred into SAFIR as boundary conditions for further thermal and structural analysis. The description of frame, localized fire and boundary conditions are described as below:

4.2.1 Frame and Sections

A 2-bay 3-storey frame is defined for this study. The dimensions and section sizes of beams and columns are mentioned in the table below:

Table 1 Geometrical properties of sections used

Section Properties	Column	Beam	Geometry
Type	Cold-formed square hollow section	Universal beam	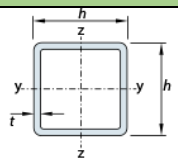 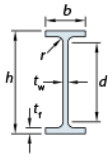
Depth (mm)	80	76	
Height (mm)	80	127	
Thickness (mm)	3	--	
Web thickness (Tw)	--	4	
Flange thickness (Tf)	--	7.6	
Surface area	0.310	0.310	
Weight	7.07	7.07	

The frame consists of beams spanning 4m and the height of each column is 2m. The ground floor columns have fixed supports at the bottom. The material properties of steel are taken as per Eurocode and are tabulated in the Appendix A of thesis.

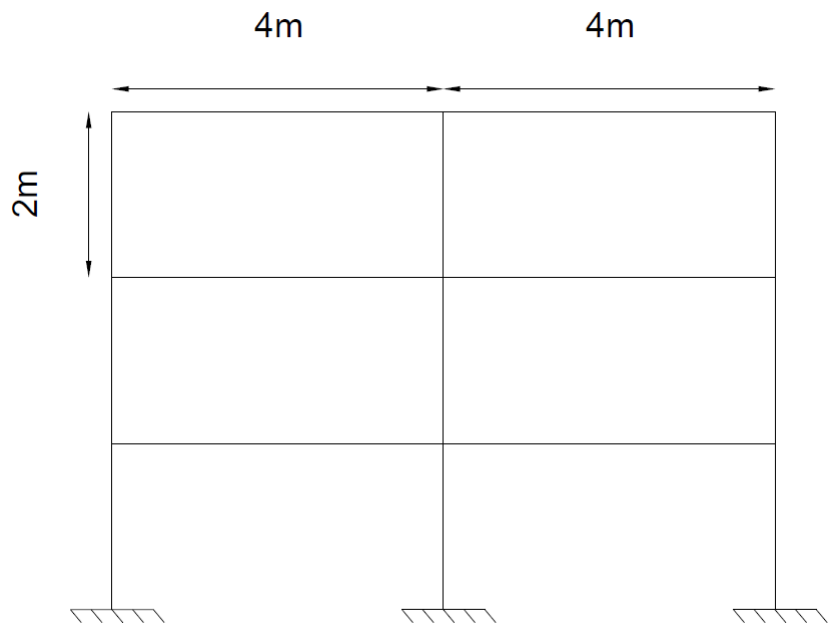

Figure 12 Frame structure for case study

Six fire scenarios are defined based on the location of the column. In each case, only one column is subjected to localized fire while the rest of the structure remains at ambient conditions.

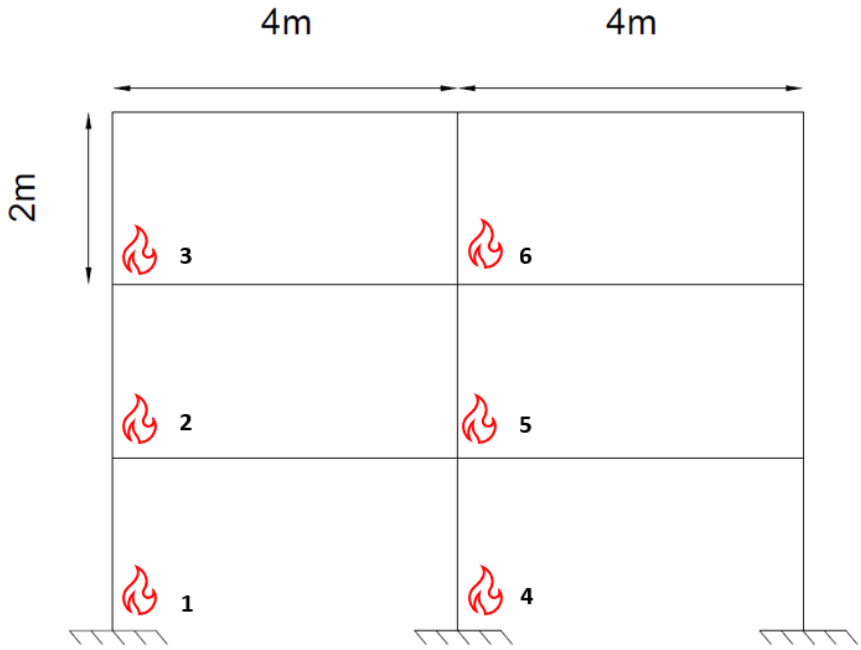

Figure 13 Six different locations of fire column under investigation

4.2.2 Fire Analysis

To obtain a real time-temperature data for a column exposed to a localized fire, a fire simulation is done in FDS. The simulation is carried out by defining a crib in front of a steel column. A prescriptive heat release rate is assigned to the crib and the material properties of Australian pine wood are taken from [49]. The reason for choosing this crib fire from literature is that the slow burning of this wood results in a higher temperature and fire load. It helps in achieving temperatures over a longer duration which are not obtained from ordinary crib fires. The properties of wooden crib are given in the table below:

Table 2 Material properties of crib used for fire simulation. Properties taken from [48].

Crib Details	Value
Density (Kg/m3)	440
Conductivity (W/mK)	0.147
Specific heat (KJ/Kg.K)	2.8
Emissivity	0.9
Soot yield	0.028
CO_Yield	0.01
HRRPUA (Kw/m2)	3675
Dimensions (mxmxm)	0.5x0.5x0.25

The temperature at steel surface is recorded using AST devices on each face. The simulation is run for 90 minutes at a mesh resolution of 50mm. The simulation geometry and fire development at 1000 seconds is shown below in the pictures.

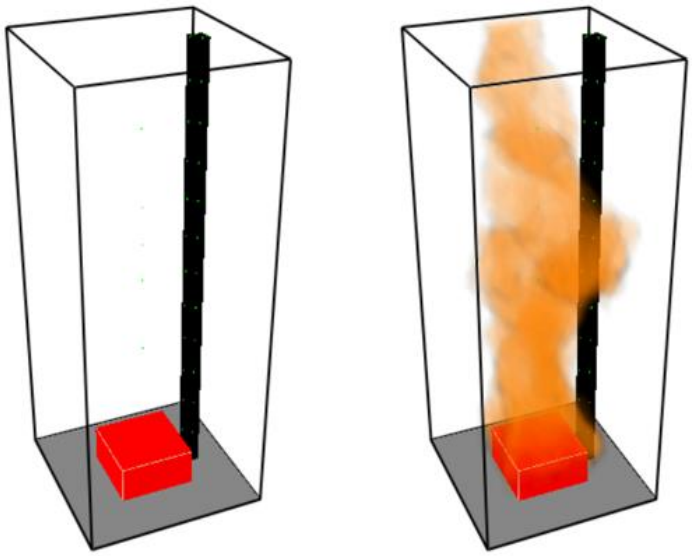

Figure 14: Geometry of fire simulation. Fire simulation at 1000 seconds.

The heat release rate obtained during the simulation is closer to the prescribed data and was not improving with a finer mesh therefore, a mesh size of 50mm is chosen because of less computation time and power utilization.

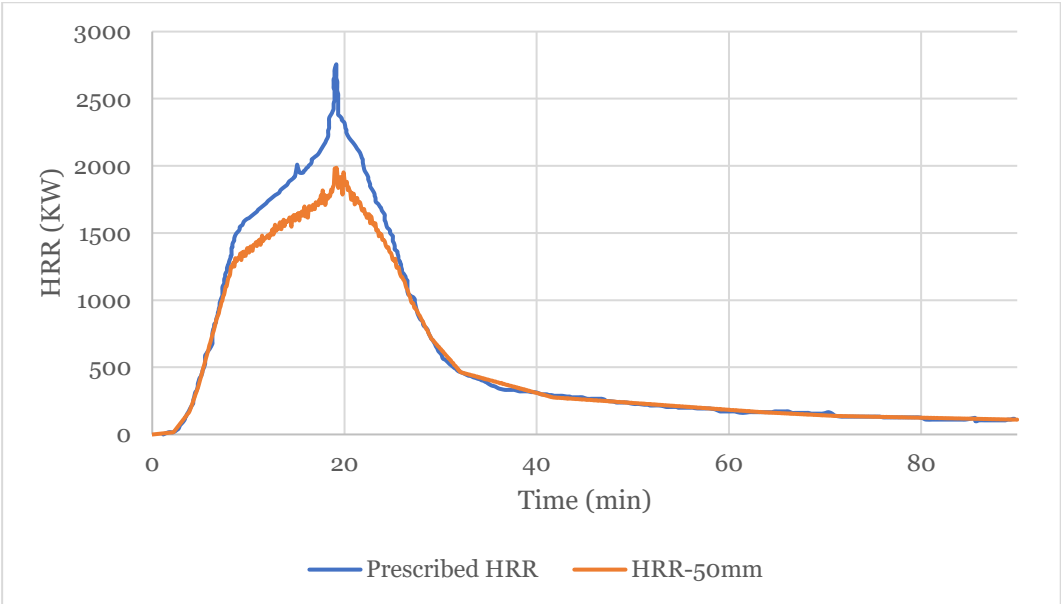

Figure 15: HRR comparison obtained from FDS and literature.

4.2.3 Thermal & Structural analysis

The AST data obtained from the FDS simulation was applied as frontier boundary condition on 2-D steel sections. The steel column was applied 4 different AST files at intervals to obtain a realistic temperature on the surface. More details about applying AST files on steel are described in the validation section of thesis.

The loads are defined for the frame in such a way that the central ground floor column is at 65% of its maximum load carrying capacity at ambient temperatures. The side columns of the frame are loaded at 30% of their maximum capacity. Uniformly distributed loads are applied on beams. Loads applied are mentioned in the table below:

Table 3: Loading conditions applied on the frame.

Members	Location	Loads (KN)
Columns (Point loads)	Ground floor	15
	First floor	15
	Second floor	10
Beams (Uniformly distributed)	Ground floor	8
	First Floor	8
	Second floor	4

5 Results

The results from the validation study and the case study for progressive collapse mechanism are presented in this section.

5.1 Validation Study

5.1.1 Thermal response

To meet the first objective of the validation of SAFIR in terms of thermal response. The adiabatic surface temperature is imported from FDS into SAFIR, the steel section is investigated at specific locations and the time-temperature data is obtained. The general overview of the temperature distribution throughout the structure is shown below. Temperature distribution in the 3-D model is visualized in post-processor software Diamond. The figures below show the temperature distribution at 1 hour and at 2 hours of the simulation time.

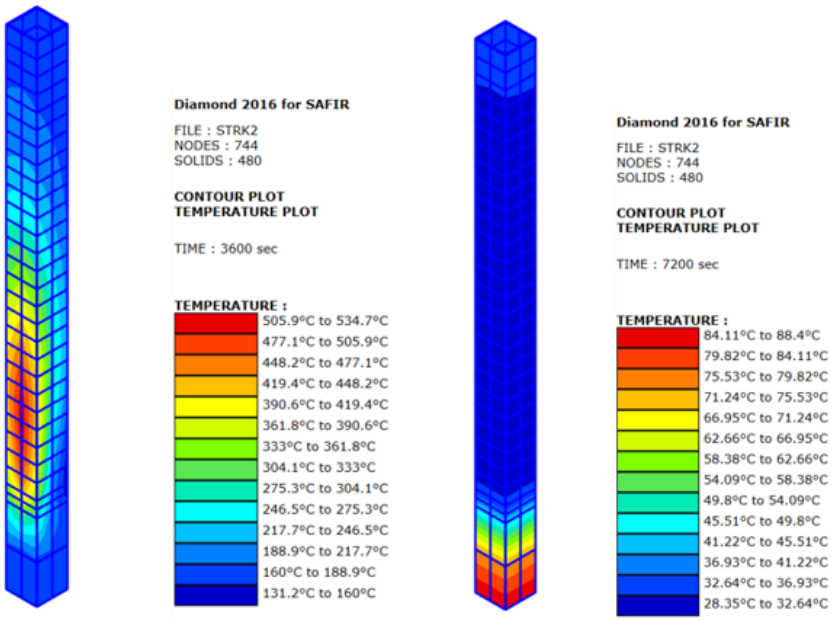

Figure 16: Temperature distribution in 3-D Steel section at 1 hour and 2 hours of simulation

Temperature distribution at different heights on the steel column is compared with the reported results from the experimental scheme. First, the temperature on the front surface and corner at the height of 0.4m is compared. The temperature at the side and back surface are compared at 0.6m from the base. The results obtained from this comparison are presented below:

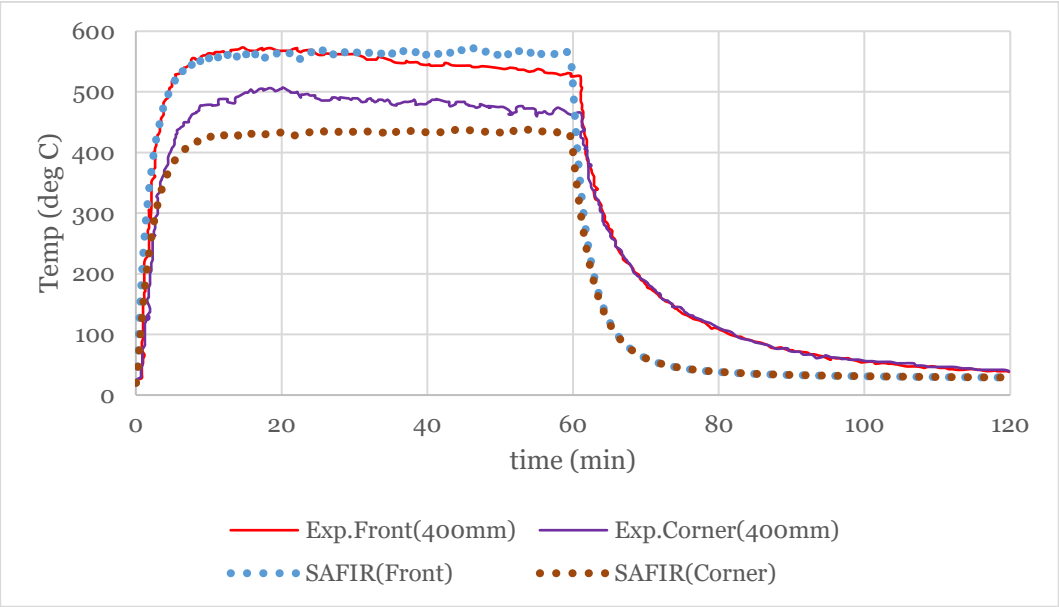

Figure 17: Comparison of steel temperatures at front face and corner (z=400m) in 3-D thermal analysis

As can be seen from the graph above, the temperature predicted by SAFIR at the front face of the column at 400mm is quite close to the experimentally measured data. SAFIR underpredicts the temperature for initial 27 minutes by approximately 1.27%. At 27 minutes, the temperature in SAFIR is 562.8 °C while the experimental data reported 562.42 °C. This shows that the measurements of SAFIR are in good relation to the experimental data. However, after 27 minutes, SAFIR starts to overpredict the temperatures by approximately 2.98% until 60 minutes. At 60 minutes, the fire is extinguished, and the temperature has dropped rapidly. At 59.9 minutes, just before the extinguishment of fire, SAFIR has 563.61°C while experimental data reports 522.1 °C. After 60 minutes, SAFIR seriously underestimates the cooling phase temperature on average by 48.6%. This could be because of the change of emissivity of steel and surrounding conditions in real test while SAFIR idealises some parameters and an ideal rapid cooling phase is yielded.

At the corner, SAFIR temperatures are on average 11.68% lower than the experimental data for the first 60 minutes of fire. After 60 minutes, when the fire is extinguished, the underestimation of steel temperature is by 48.6% by SAFIR. The temperature distribution in steel at the side and back surface is measured at 0.6m from the base of the column. The results from SAFIR are compared with the experimental data in the chart below.

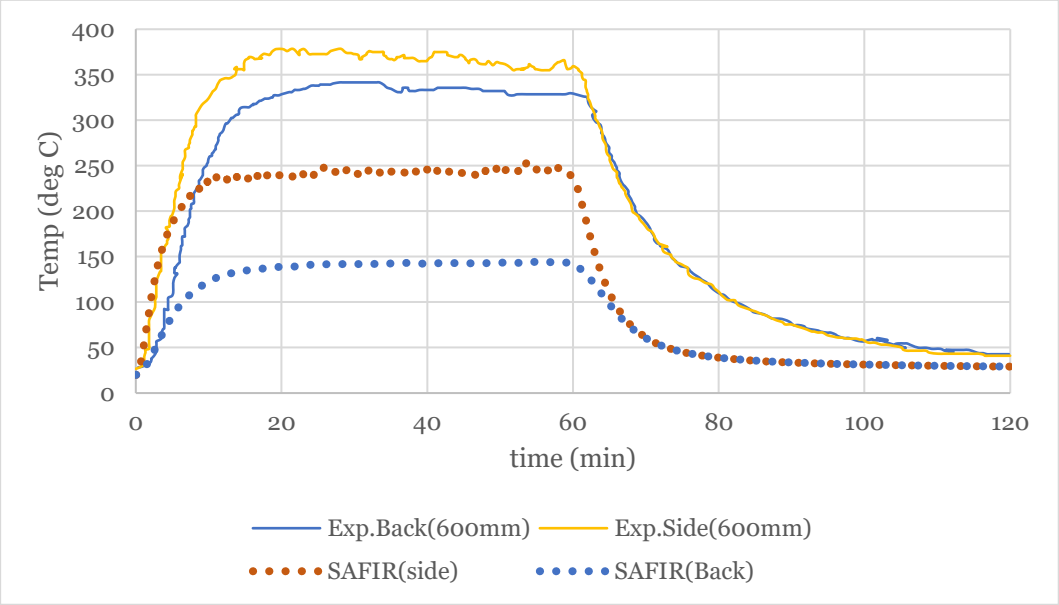

Figure 18: Comparison of steel temperature at the side and back surface (z=600mm) in 3-D thermal analysis

The temperature reported by SAFIR on the side and back surface is much lower than the experimentally reported data. The temperature at the side surface predicted by SAFIR is 33.3% lower for the first 60 minutes. After 60 minutes, SAFIR underestimates by 48.4% as compared to the experimentally reported results. Similarly, the temperature at the back surface of the steel column is approximately 56% lower in SAFIR for the first 60 minutes. After the extinguishment of fire, the temperature difference is 50% up to 120 minutes. The temperature difference is much larger than the expectations and the authors have tried to investigate the reasons in the next section.

This difference in the results is presented below in the form of a table.

Table 4: Summary of SAFIR 3-D analysis results compared with the experimental data

Location	**Height**	**Time duration**	**% Difference**	**SAFIR-estimate**
(Face of Column)	(mm)	(minutes)	(Average)	(Compared to experimental)
Front	400	0-27	1.27	Under
		27-60	2.98	Over
		60-120	48.6	Under

Corner	400	0-60	11.68	Under
		60-120	48.6	Under
Side	600	0-60	33.3	Under
		60-120	48.6	Under
Back	600	0-60	56	Under
		60-120	50	Under

The above tabulated data is also presented in the form of chart below:

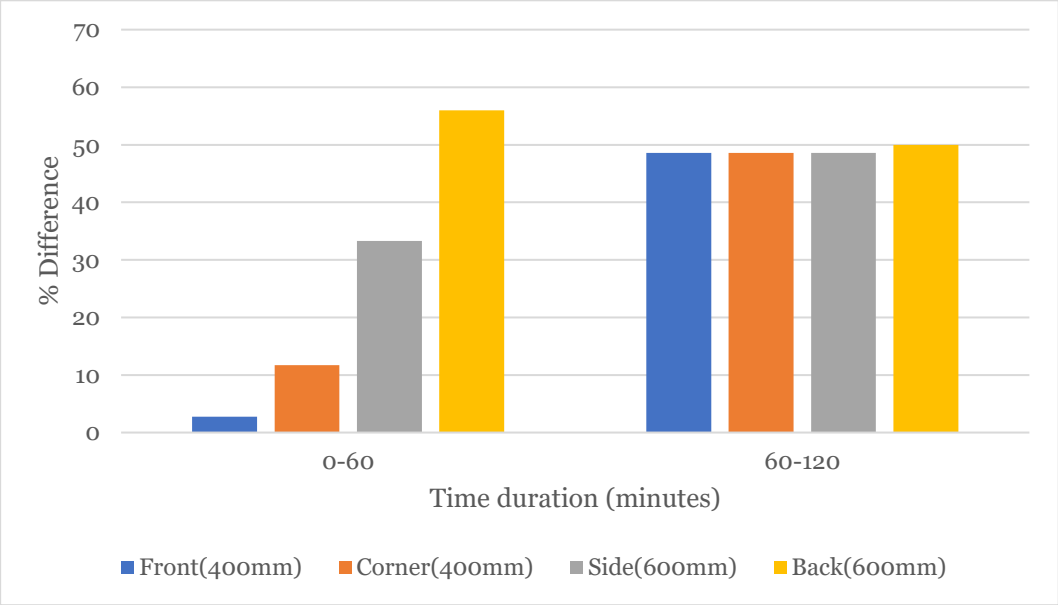

Figure 19: Average % difference in the temperature calculated by SAFIR and experimental data

Inspection of inaccuracy

The temperature differences are much higher than the anticipated results, especially on the side and back surfaces. The reason for this inaccuracy can be explained by assuming a single steel section of 0.1m x 0.1m.

The steel column (STRK) under investigation is a hollow section. At elevated temperatures, when the temperature distribution is non-uniform at each face, there will be a transfer of heat inside the hollow section. The front face of the column is facing higher temperature due to the flame front, therefore; the back surface of the front plate will have theoretically the same temperature as the front surface. The air inside the cavity will also get an increase in temperature due to convection and radiation from the inner side of the front plate. The air inside the void will get heated and will act as a medium of heat

transfer from the front plate to the backplate of the steel column. Therefore, it is obvious that the heat transfer from the front plate to the backplate is not only through conduction but also via convection and radiations. It is illustrated in the figure below:

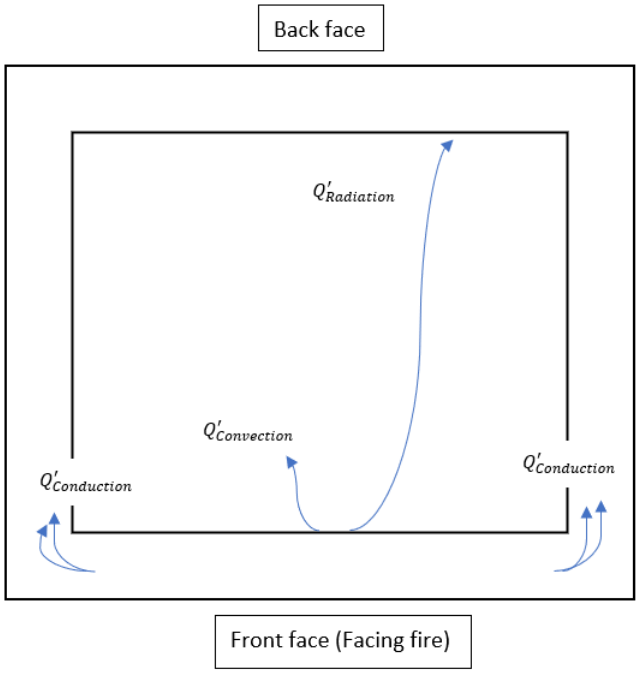

Figure 20: Heat Transfer inside the cavity of Hollow Steel section

SAFIR is capable of calculating heat transfer through cavity but only for 2-D thermal analysis. In 3-D thermal analysis, SAFIR does not incorporate the heat transfer via the internal cavity in its calculations. Therefore, the temperatures predicted by SAFIR at the side and back surface are much lower than the experimentally reported data.

2-D Thermal Analysis

The above argument is reinforced by redoing the thermal analysis for the hollow steel section in SAFIR 2-D thermal analysis. This time, the void is specified at the internal side of the section and therefore, SAFIR will incorporate the energy transfer due to convection and radiation through cavity. The section is modelled in 2-D and the frontier boundary conditions are assigned in the form of temperature files obtained from the CFD analysis. The AST files at z = 400mm, 600mm, 800mm and 1200mm are taken from the FDS device output and one file is assigned to each face of the column. Internal void is specified as a 'Void constraint' and is assigned to the internal steel section. Material is kept the same as specified earlier. The material properties are

taken from Eurocode and are specified in Appendix A. After analysis, the output files are visualized in the post-processor Diamond.

The temperature distribution at one hour and two hours of fire exposure is illustrated in **Figure 21**.

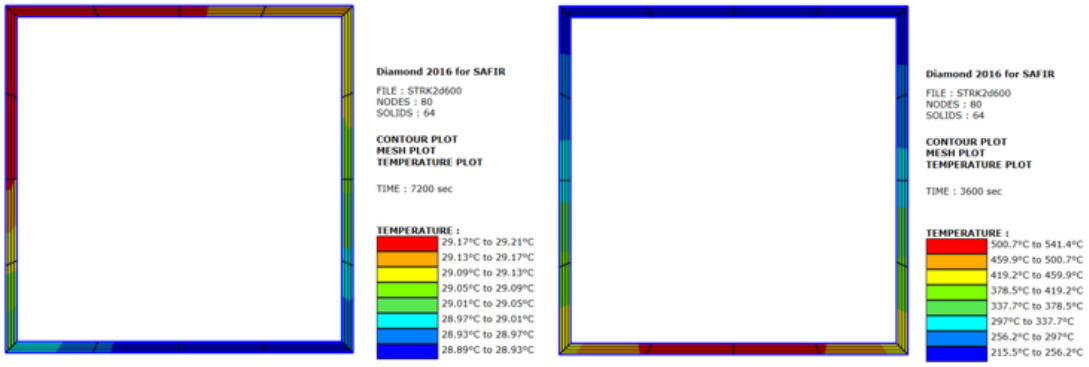

Figure 21: Temperature distribution in the 2-D thermal analysis at 1 and 2 hours of fire exposure.

The temperatures measured at the front, corner, side and back faces of the column at various heights (400mm, 600mm, 800mm and 1200mm) are shown in the graph below:

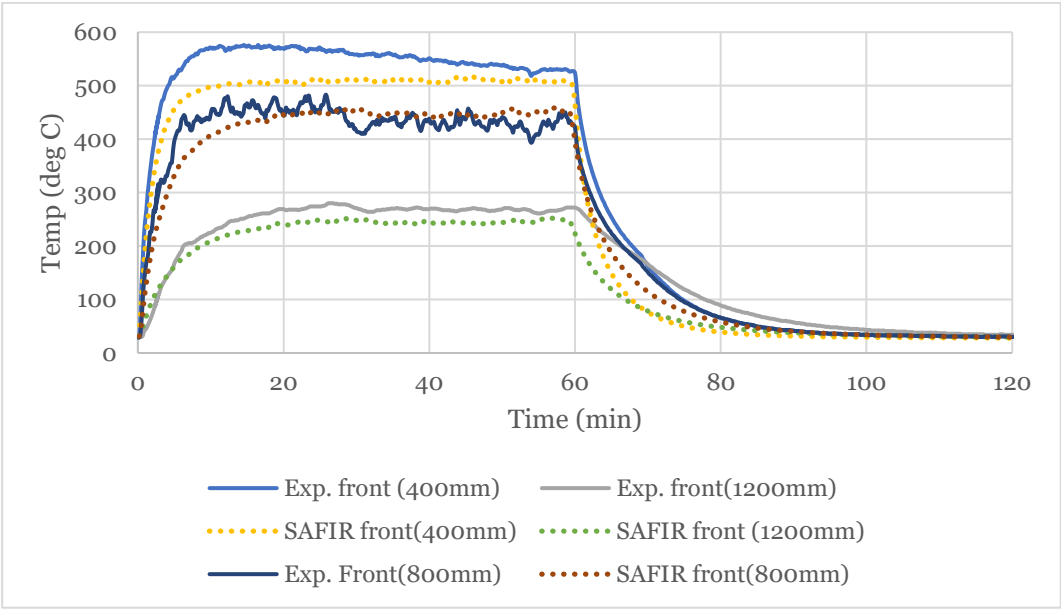

Figure 22 Comparison of steel temperatures at front face at various heights

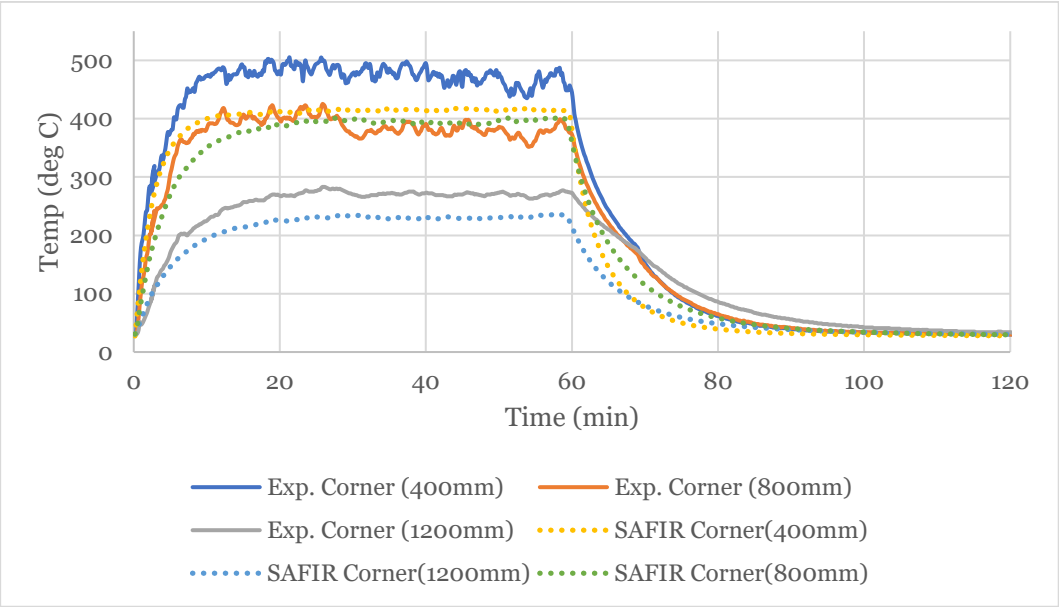

Figure 23 Comparison of steel temperatures on the corner at various heights.

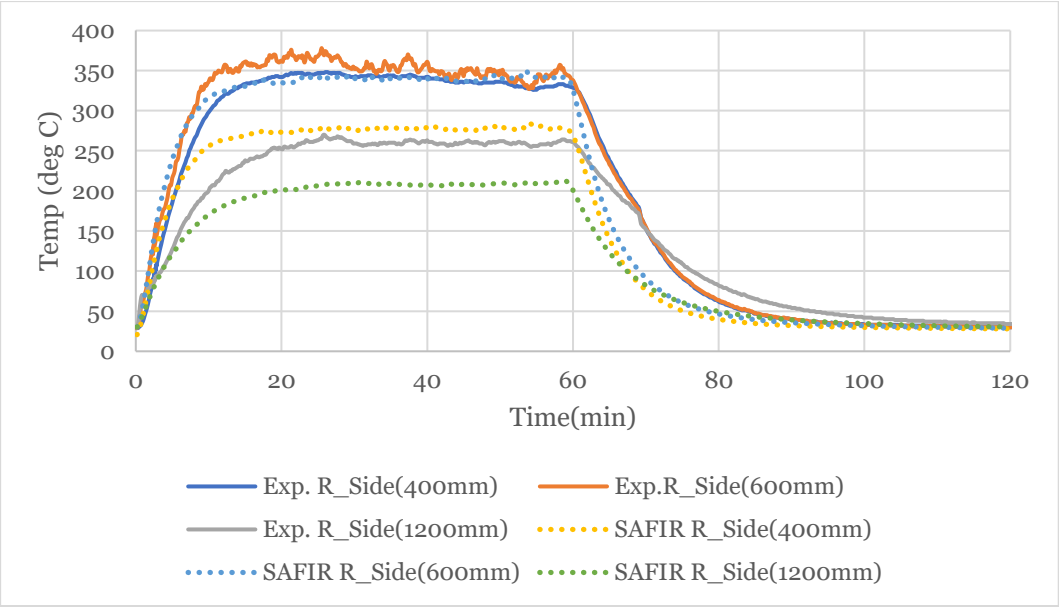

Figure 24 Comparison of steel temperatures on the side face at various heights

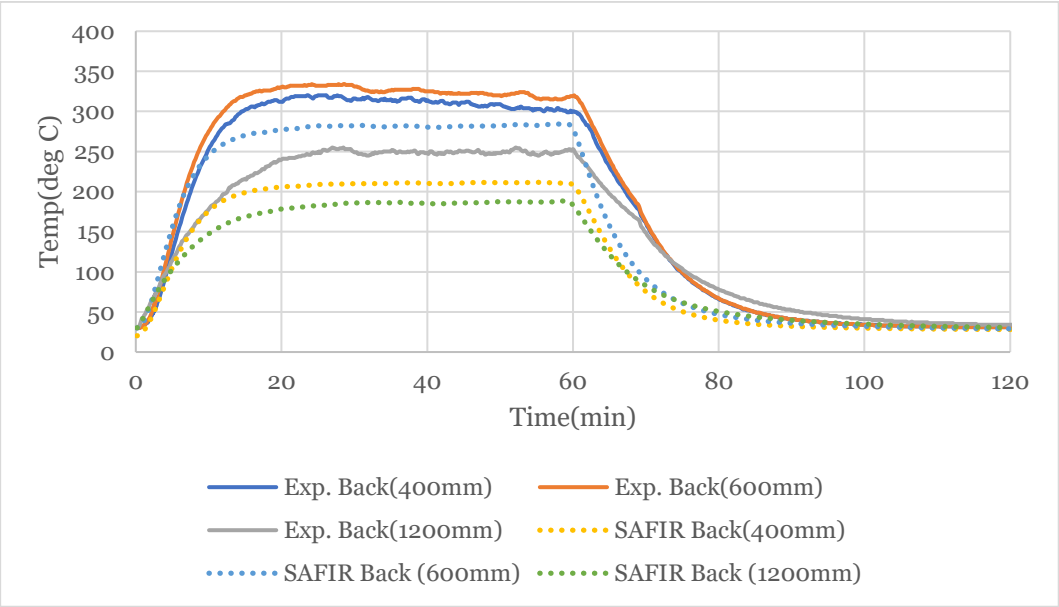

Figure 25 Comparison of steel temperatures on the back face at various heights.

It is found from the graphs above that the 2-D thermal analysis in SAFIR has calculated more accurate results as compared to the 3-D thermal analysis. The definition of void has resulted in higher temperature at the side and back surfaces. SAFIR has calculated the heat transfer due to convection and radiation inside the hollow steel section. The difference of temperatures obtained with 2-D thermal analysis are tabulated in the Appendix B of thesis.

At the back face, the temperatures measured are still not very accurate. The reason could be that the SAFIR is not taking into account the transfer of heat from the bottom plates due to the limitation of 2-Diminsional analysis. However, a sensitivity analysis is done to find out the parameters influencing the results.

Sensitivity Analysis

A sensitivity analysis is done to find out the difference of temperature at the side and back surfaces. Authors have found that the SAFIR analysis is using the standard values of convective heating coefficient, convective cooling coefficient and the emissivity of steel. However, the default values of these parameters used in SAFIR are valid for the standard fire testing [50]. In the experimental case under investigation, choosing the standard values may be the cause of this difference in temperatures. Therefore, the values for these coefficients are changed and the difference of temperatures is measured.

Four different set of values are chosen for the convective coefficients and emissivity of steel and the results are compared at the height of 600mm.

Table 5 Parameters for sensitivity analysis

Parameters	Convective Coefficient Heating	Convective coefficient cooling	Emissivity
Default SAFIR	25	4	0.7
S1	15	4	0.7
S2	25	9	0.7
S3	25	4	0.9
S4	15	9	0.9

By increasing and decreasing the values of convective coefficients, the temperature development on the back face of the column varies. It has been found that the back face temperature is close to experimental results when the convective heating and cooling coefficients are taken as 15 and 9. The emissivity of steel is taken as 0.9. The reason behind this difference is that the back face of the steel is not exposed to fire and the temperature elevation occurs slowly. Similarly, the cooling happens fast when the fire is extinguished. The comparison of four cases in sensitivity analysis with the experimental data is shown below.

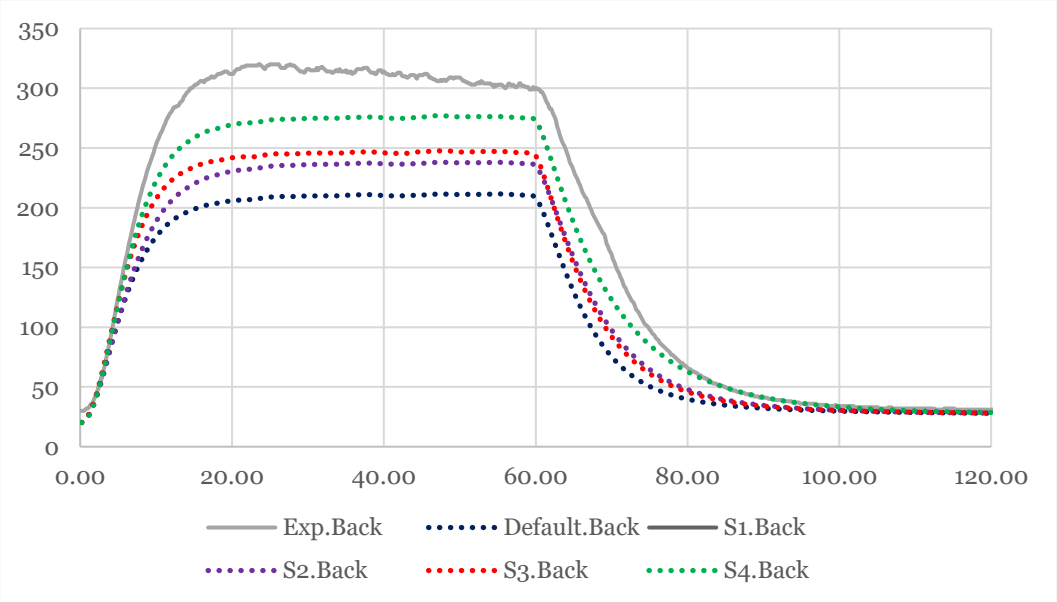

Figure 26 Variation at back surface temperature in sensitivity analysis

5.1.2 Mechanical response

Mechanical response of column is calculated in SAFIR using the problem type 3-D structure. Column is divided into four sections as mentioned in section 0. A structured mesh is built by assigning 20 numbers to the column section. It resulted in 80 beams of equal length and a total of 166 nodes. The nodes taken for comparison in SAFIR are not exactly at the same height however, they are very close to the points at which experimental data was reported. For example, the lateral displacement was measured at 775mm in experiments while the SAFIR node at 767.5 mm is taken for comparison. The column section along with its displaced configuration at 60 minutes of fire exposure is shown as:

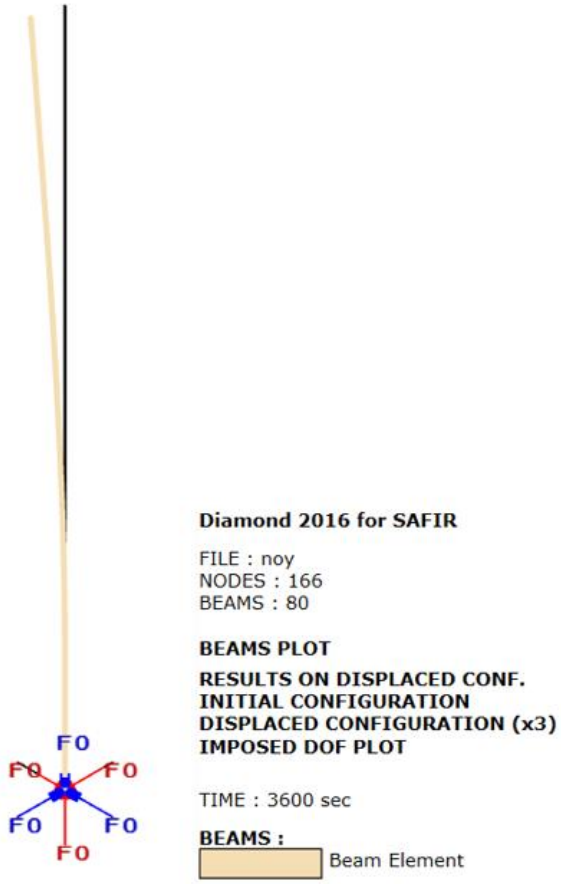

Figure 27: The displaced configuration of the column at 1 hour of fire exposure.

Horizontal displacements

As described in [43], the structural response of the column is reported in the form of horizontal and vertical displacements. Horizontal displacement is reported at five different locations along with the height of the column. The results from SAFIR structural analysis compared with the experimental data are illustrated below:

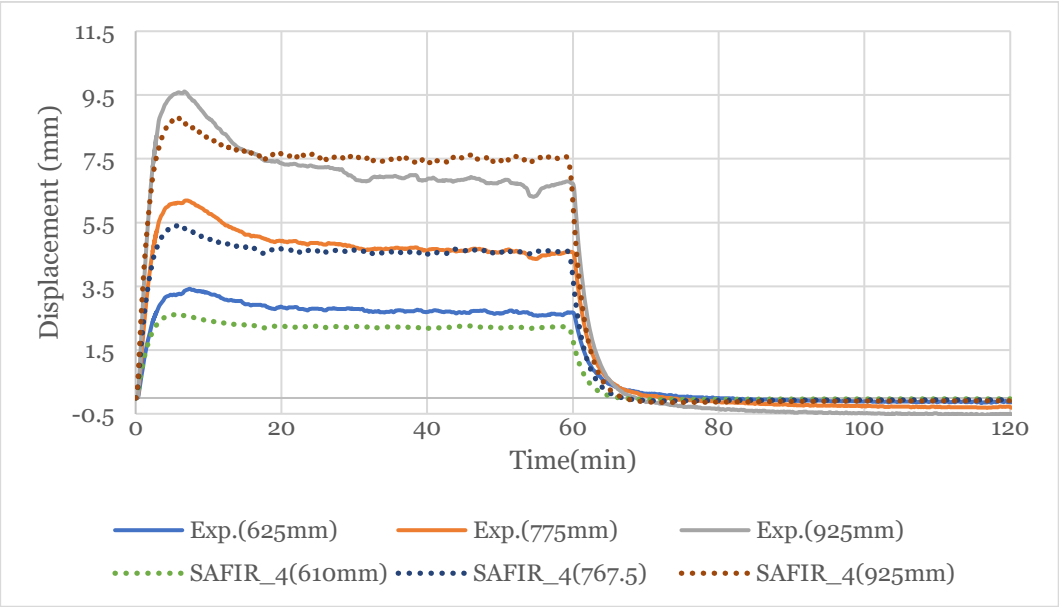

Figure 28: Comparison of horizontal displacement at z=625mm and z=775mm.

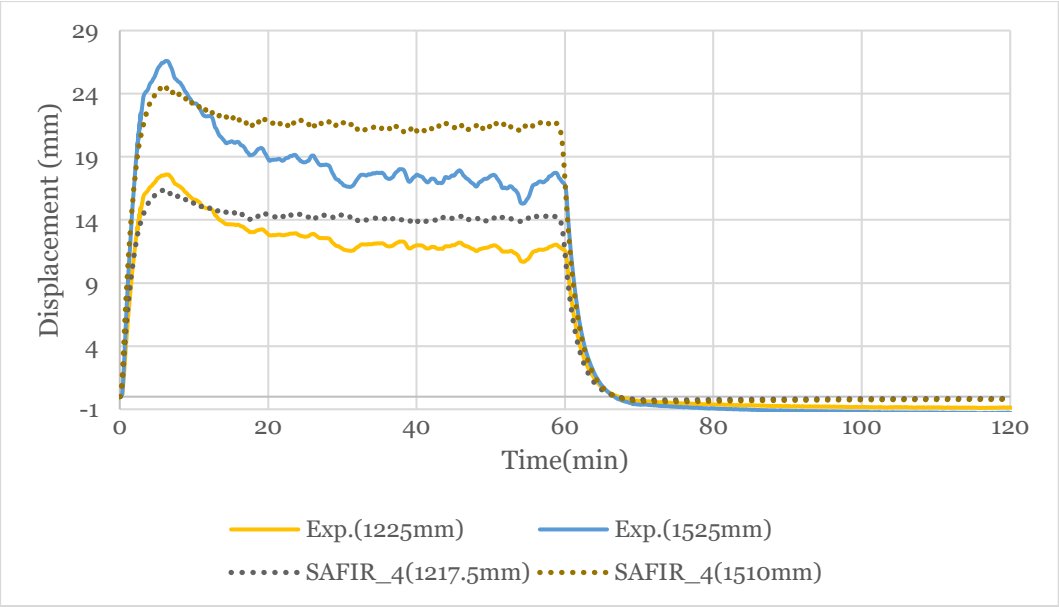

Figure 29 Comparison of horizontal displacements at z=1225mm and at z=1525mm.

As it can be seen from the above graphs that SAFIR calculates horizontal displacement very accurately and the data is consistent with the experimental results. However, the displacements measured by SAFIR show difference at various points. The peak measured displacement is lower than the experimental data. After the maximum displacement, SAFIR reports uniform value for the duration of the fire. On the other hand, experimental data reports decrease in displacement after the peak measured value.

Vertical Displacements

The vertical displacement is compared at the height of 1225mm in the experimental data. The comparison of the vertical displacements calculated by SAFIR at the height of 1217.5mm with the experimental data is illustrated in the graph below:

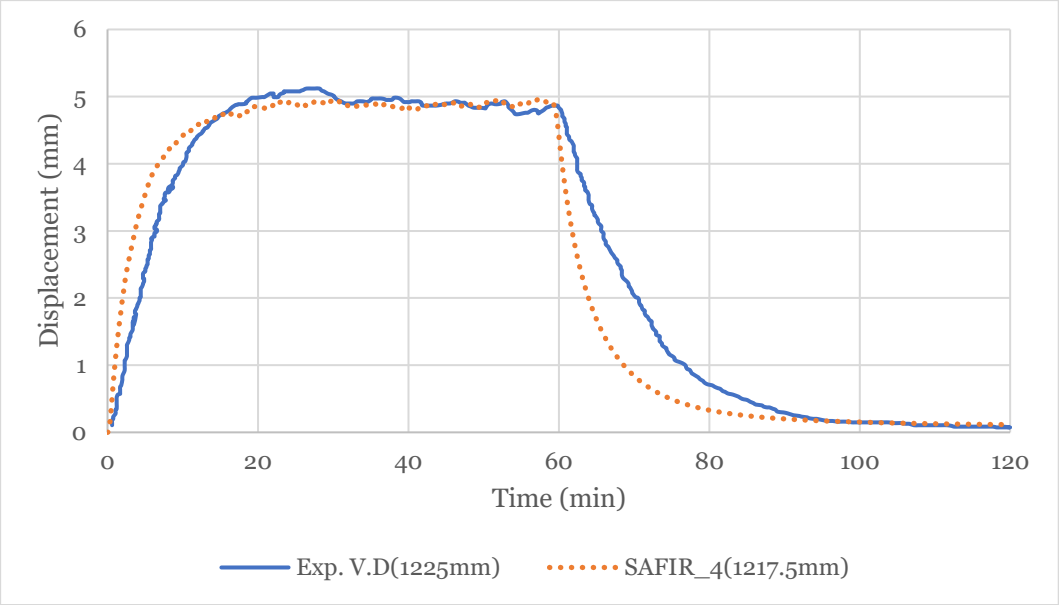

Figure 30 Comparison of vertical displacement at z = 1225mm.

As can be seen from the graph that SAFIR measures vertical displacement very close to the experimental data. The displacement measured by SAFIR at the start of the heating phase is rapid and the decrease in displacement is also rapid during the cooling phase.

The average difference between the measured values is illustrated in the graph below:

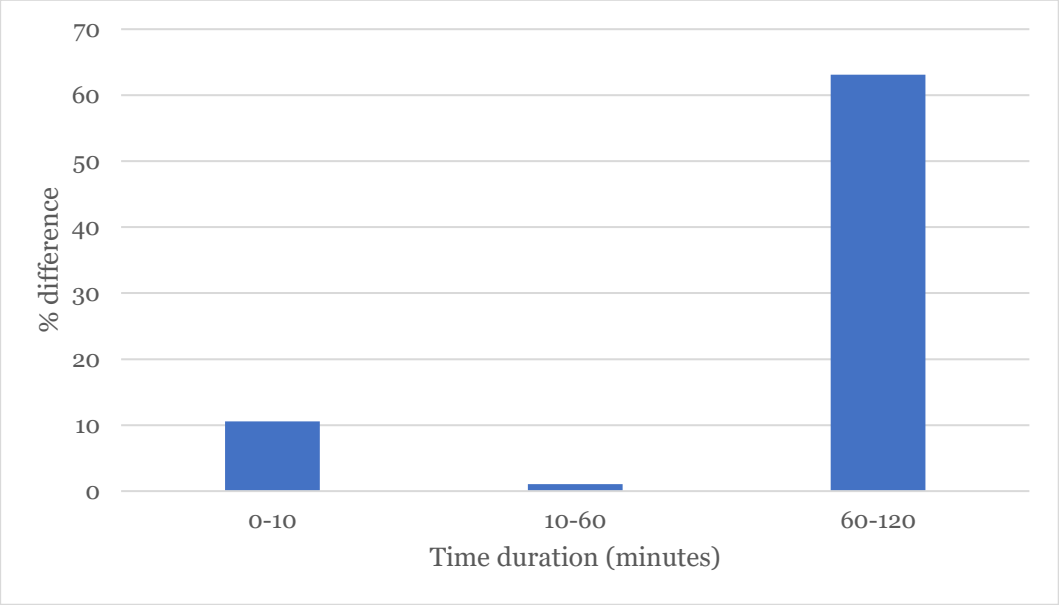

Figure 31: Average % difference in the vertical displacement.

Sensitivity Analysis

As reported in the methodology section 0, authors tried to find out the effect of dividing column into several sections. Another structural analysis is carried out where the column frame is divided into 15 sections. Each section is run in thermal 2-D analysis by applying AST-surface time-temperature curve. A total of 60 AST files were extracted from FDS. The column mesh resulted in 300 number of linear elements and a total of 616 nodes.

Dividing column into more sections and applying more AST-files result in slightly different horizontal and vertical displacements results. Theoretically, running simulation with more AST-files should result in accurate displacements however, the results suggest that sometimes it is more accurate with less input data from CFD. The horizontal displacement measured by applying 4 AST file and with 15 AST files is illustrated in the graph below:

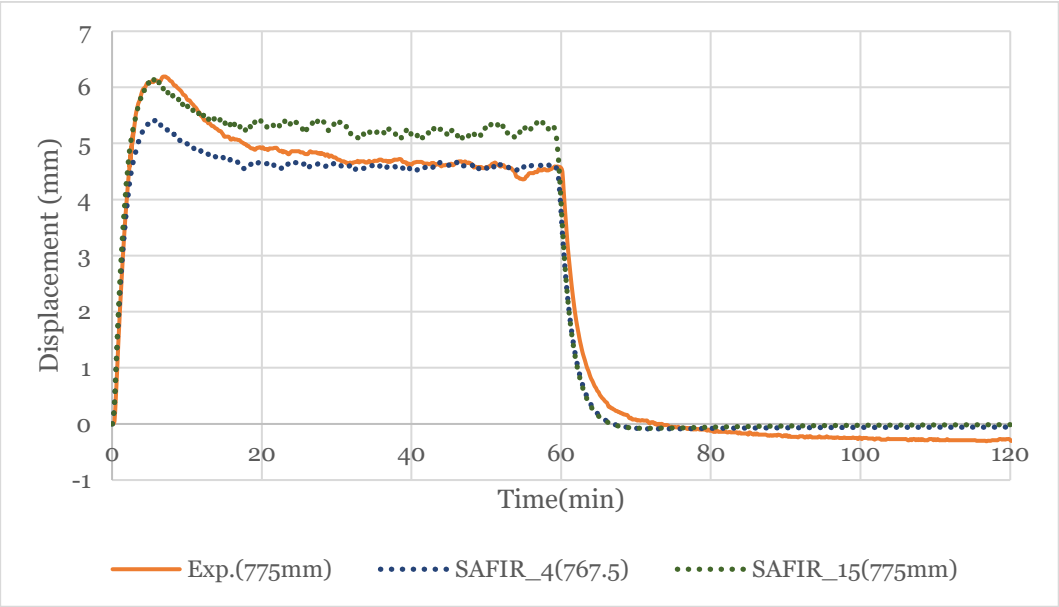

Figure 32 Comparison of horizontal displacements measured using 4 and 15 thermal output files.

As it can be seen that the applying 4 AST data files results in lower peak horizontal displacement at 775mm height of column. However, the average displacement agrees with the experimental data. On the other hand, using 15 AST files result in accurate peak displacement value but an overprediction during the fire duration. This trend is not consistent at different heights and therefore it cannot be concluded that if using more AST-files results in accurate displacement measurements. Similarly using more AST files data results in underprediction of vertical displacements of the column.

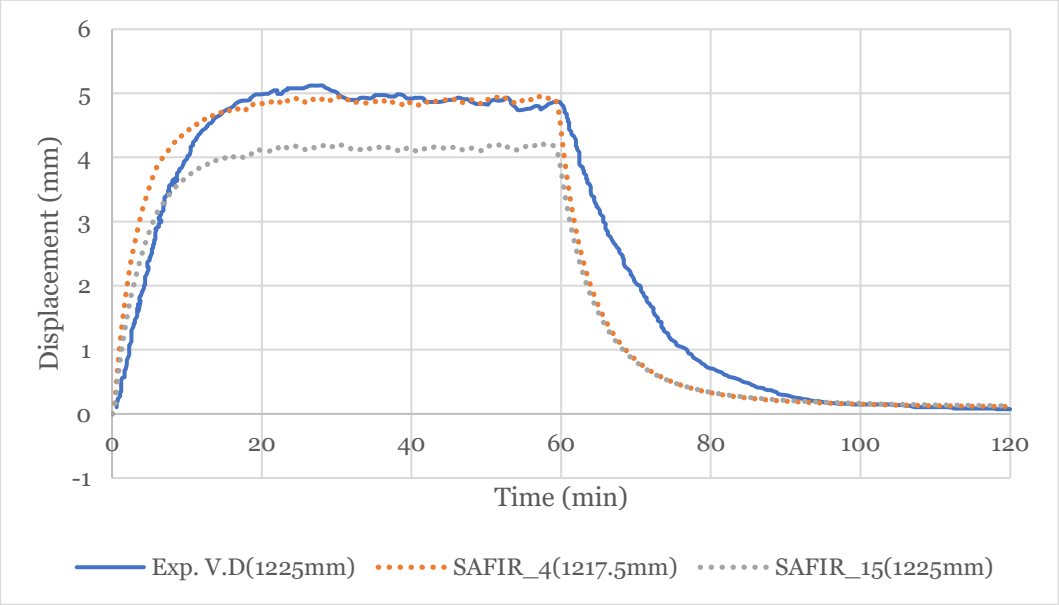

Figure 33 Comparison of vertical displacement by using 4 and thermal output files.

The comparison of accuracy obtained based on the number of AST-files extracted from CFD and assigned in SAFIR is illustrated in the form of table below:

Table 6 Accuracy achieved at different height based on the number of thermal output files in structural model.

Height (in mm)	SAFIR_4	SAFIR_15
625	✓	
775		✓
925	✓	
1225		✓
1525	✓	

5.2 AST vs AST-gas

AST-gas devices are applied exactly at the same locations where the AST-surface devices were applied in the first simulation. Time-average values of temperature are plotted over the height of the column and this graph is compared with the time-averaged temperature from AST-surface data and the data reported by [42]. The reason is to understand the difference in temperature between AST-surface device and AST-gas device.

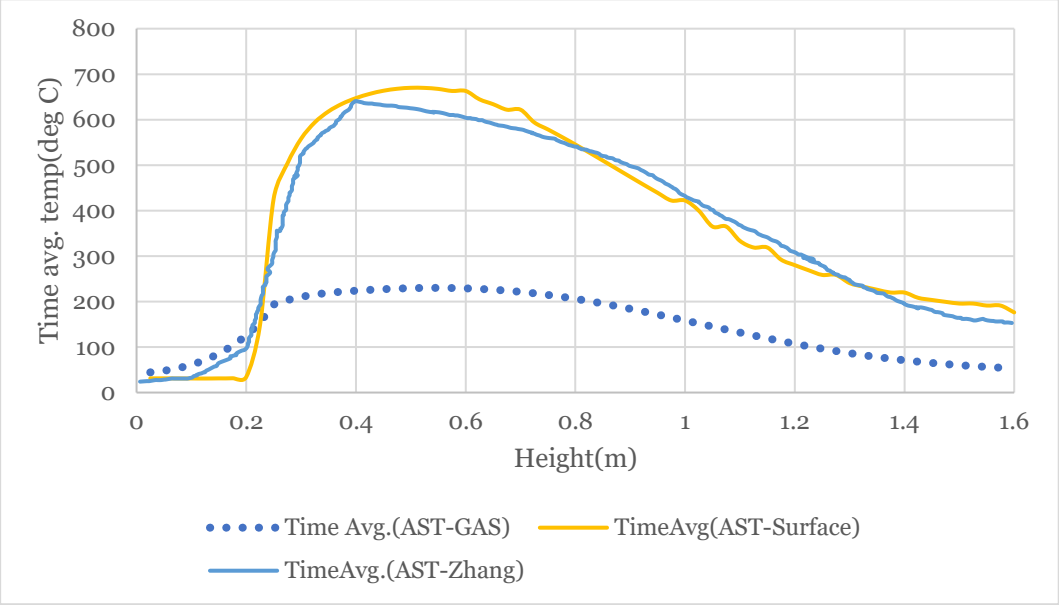

Figure 34:Time-average comparison of temperature obtained by two devices and reported in literature.

As it can be seen that the time averaged temperature measured by the AST-gas device is much lower than the temperature measured by the AST-surface devices. The reason is that the AST-gas measures the gas temperature however AST-surface device measures the temperature obtained by the steel column due to incoming energy from the burner. As the steel column is in close proximity of the burner, the flame and temperature development is influenced and absence of obstruction geometry will result in recording of only gas temperature which is lower.

As it was previously reported by [19], applying AST-gas device in FEM packages seriously underestimates the temperature development. This can be seen in the graph below:

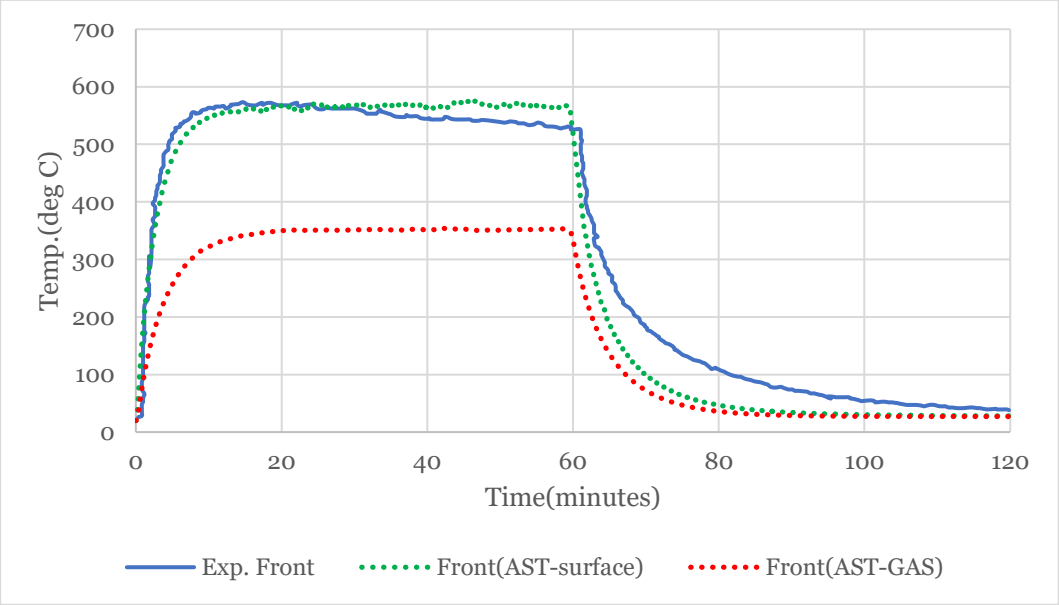

Figure 35: Comparison of front surface temperature obtained by AST-surface and AST-gas device.

Since the AST-gas device is seriously underestimating the temperature development in the steel section, therefore, further thermal analysis on the back and side surface is not carried out. Similarly, the 3-D structural analysis is not done using AST-gas device time-temperature data.

5.3 Progressive collapse mechanism

The results from the case study are presented in this section. The fire analysis is done in FDS, and the frame is assigned with a column subjected to a localized fire as described in the methodology section.

The axial forces on the frame structure at ambient conditions are illustrated below. At ambient conditions, the loads are redistributed from top members to the bottom. Most of the elements are under compression except ground floor beams. Here, the positive forces show members in tension while negative forces are for members in compression.

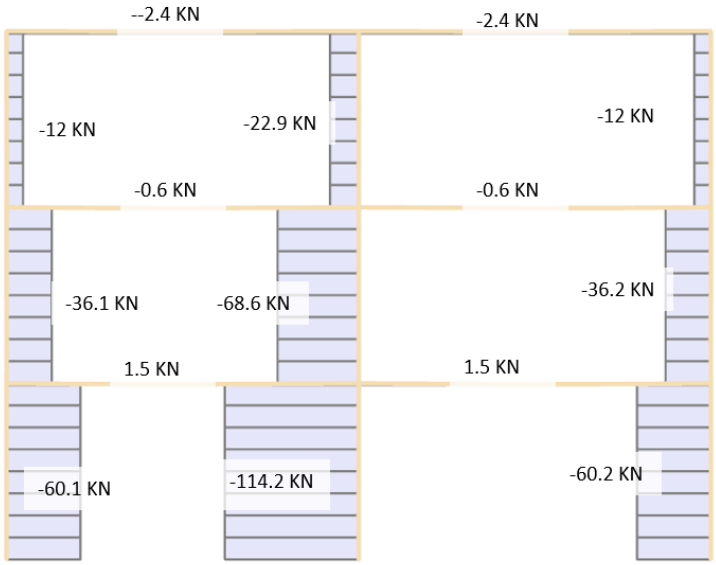

Figure 36 Axial forces in steel frame at ambient temperature.

5.3.1 Forces redistribution mechanism

When exposed to fire, heated column develops additional stresses due to its tendency to expand at high temperatures. The structural response of the frame is influenced by the expansion of one column subjected to localized fire. The column wants to expand due to increase in temperature. This elongation is restrained by the other members connected. As a result, a thermally induced compression force is added to the initial force that was being carried by the column at ambient temperatures. This leads to an unloading of the adjacent columns equal to the induced compression force. For reference, it will be referred to as stage 1.

Continued heating of the column will eventually lead to loss of strength and stiffness hence yielding, the column won't be able to carry the same loads. These extra forces will then have to be redistributed to the adjacent structural members. For reference, it will be called stage 2.

During the cooling phase, column starts to contract however due to loss of strength and material properties, it may shrink to a length shorter than its original length. This again will result in some additional stresses like tension which eventually will pull the whole frame toward itself. This stage is referred as stage 3.

Forces distribution mechanism is also dependent on the location of the fire in the structure. Positive values in the figures below present tension and negative member as compression. A scale of 10 is used to view the displaced structure in Diamond. In cases, where the whole structure collapse, a scale of 1 is used for a better view of displaced structure.

Stage 1 can be seen in the figure below:

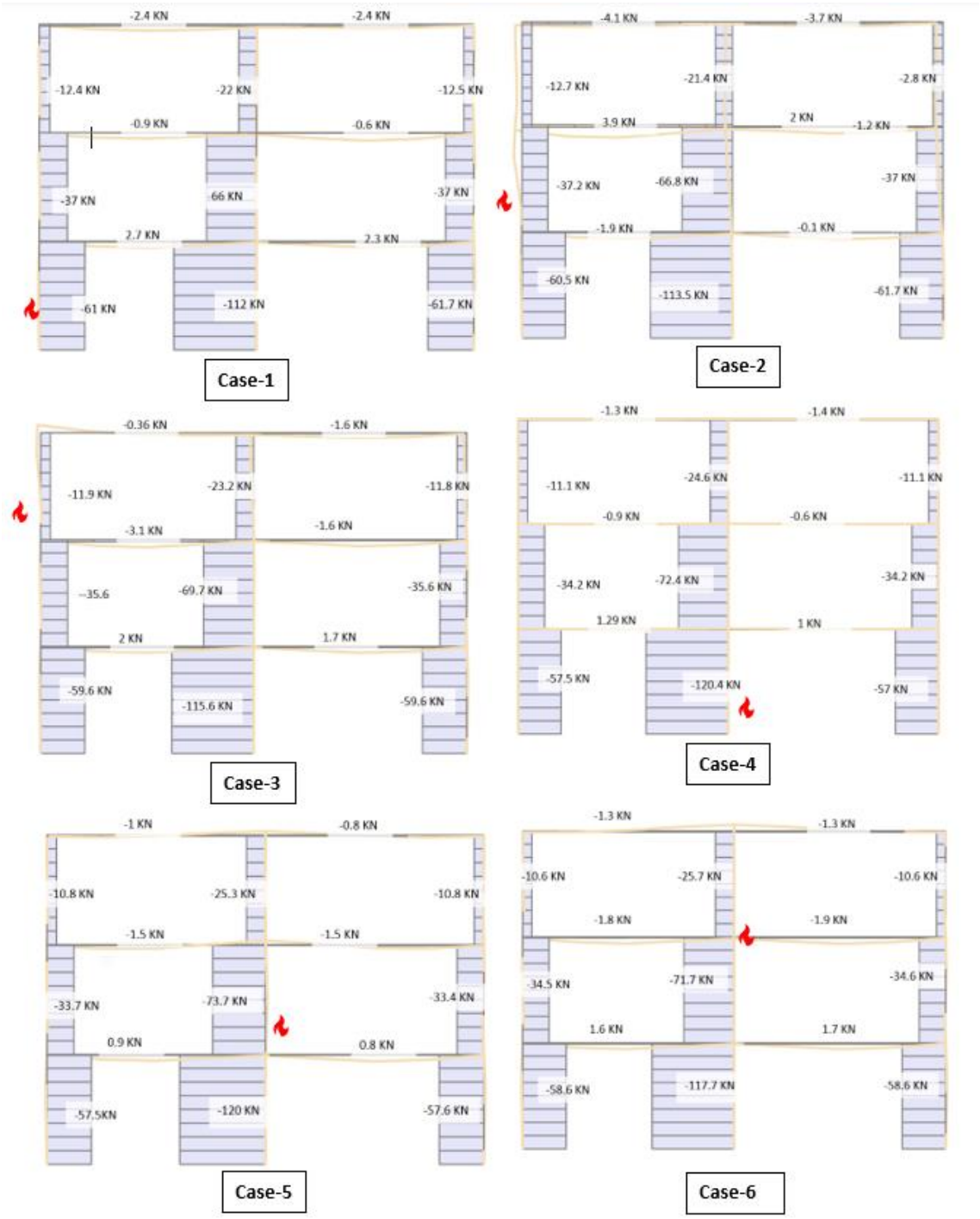

Figure 37 Forces redistribution at peak temperature of heated steel columns. Forces redistribution just before failure for case 4 and case 5.

In the figure above, in case 1, fire at the left side ground floor forces column to expand and due to restraint of fix support at lower end, it results in increased forces. These forces are then redistributed to adjacent structural members. It also results in the increased tension forces in the beams of ground floor however, rest of the structure carries similar loads as it was at the ambient temperature. The outer columns at ground floor carry slightly higher load while there is decrease in the loading of central ground floor column.

In case 2, the first-floor column exhibits similar pattern of more forces due to thermal expansion. However, to redistribute these forces, the ground floor beams which were originally in tension end up being in compression and the first-floor beam adjacent to the column go into tension while it was in compression at ambient conditions. This transition of compression members going into tension is tolerable within steel members as steel is a ductile material. However, as we know, concrete performs poor in tension, such transition of forces may be very detrimental to the safety of concrete structures.

In case 3, when the corner column at top floor tries to expand, the forces are transferred to the first and ground floor beams. Since, the member is not restrained at the top, the frame can withstand higher lateral and vertical deflections at top.

Case 4 has come out as a worst-case scenario; the frame structure collapses at 518 seconds of simulation. The forces redistribution just before collapse of structure is presented. The middle column at ground floor is critical since it is already carrying more loads than other members. Localized fire on this column results in an increase of forces. Similarly, case-5 is also a critical scenario where the frame structure collapses at 878 seconds of simulation. It also results in the increase of forces on the middle column at ground floor and first floor. However, there is also unloading of adjacent columns at the same floor. This type of behavior is called pull-in force mechanism. In a typical pull-in force mechanism, as reported by [37], an inner column is heated and the beams that are connected to it may act as catenary to redistribute the vertical load away from the heated column. This results in the increase of vertical displacements where tensions are developed in beams, and they act as catenary. An increase in the compressive forces of adjacent columns on the same floor and the floors below is observed.

In case 6, the middle column at top floor expands and exert forces on the columns below. The forces are again being redistributed to the beams on 1st floor while there is unloading of corner columns. The stage 2 and stage 3 of the load's redistribution can be seen in the photo attached below. The cooling phase of case 1,2,3 and 6 is compared to the initial loading conditions. The structure collapsed in case 4 and 5 due to the failure of heated column and eventually the collapse of whole frame.

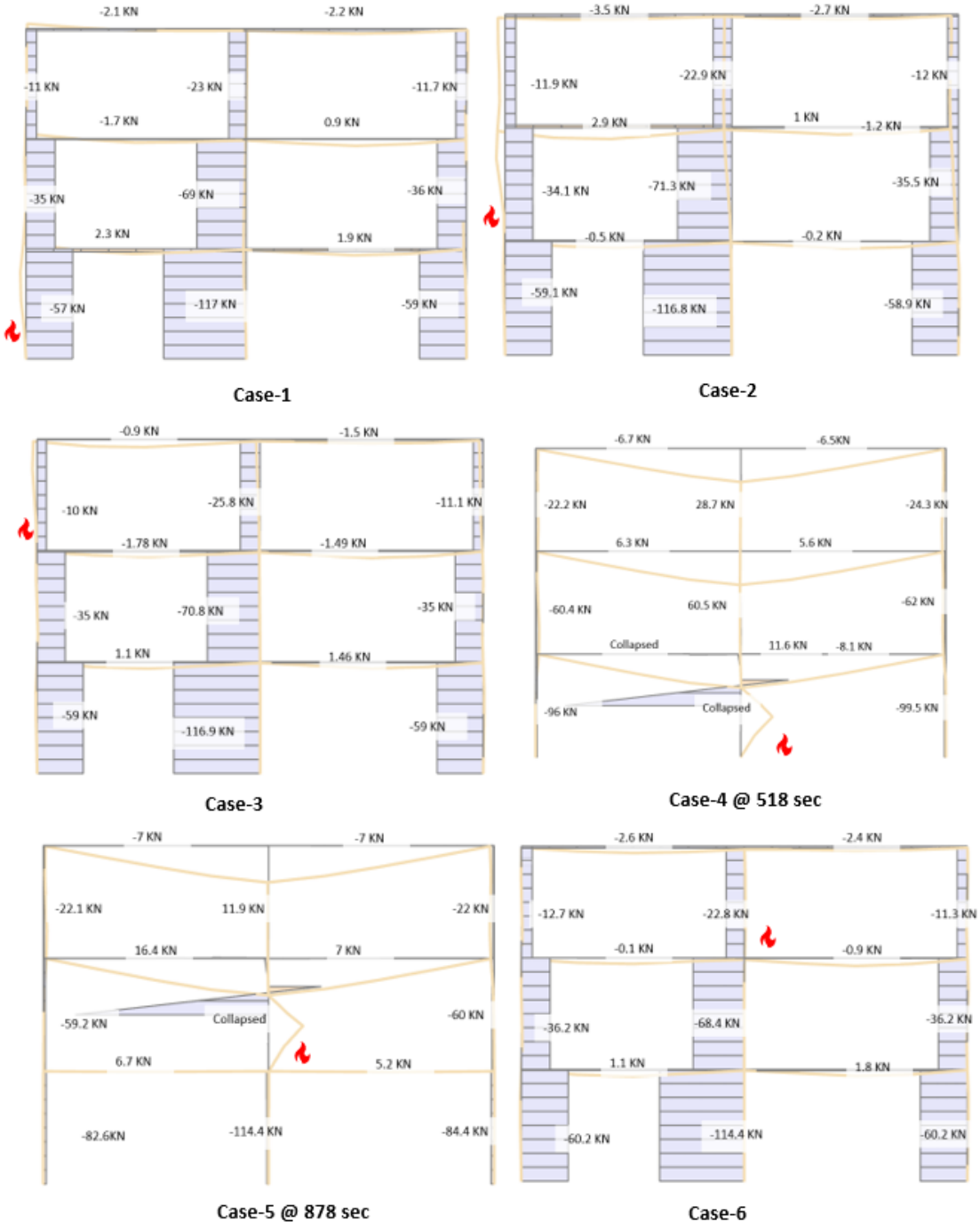

Figure 38 Forces redistribution after cooling of heated column. Collapsed structure for case-4 and case-5.

After the cooling of heated columns, forces are still being redistributed to the other structural members. It is due to the change of material properties at high temperatures and shrinkage of steel to the length shorter than its original length. The heated member results in carrying lower loads than at ambient conditions.

In case 1, at the end of simulation at 180 minutes, the corner column at ground floor carries less loads and the beams of ground floor end up in more tension than in original condition. Similarly in case 2, the beams of first floor which were originally in compression end up being in tension. One beam at right bay of frame ends up having tension at one end and compression at the other. This type of development of both tension and compression forces are detrimental to a member and has significant effect on the performance. This is called cantilever beam mechanism. The upper half of beam is subjected to tensile stresses, tending fibers to elongate while the lower half to compressive forces, forcing them to crush. Same is the situation with case 3, heated member ends up carrying less forces after cooling and the adjacent members carry more.

5.3.2 Failure mechanism

The column in case 4 fails at 518 seconds and results in the failure of whole structure. The stresses in the column exceed its maximum load carrying capacity at elevated temperature and it redistributes the forces to side beams and columns. There are two failure mechanism observed in this case. First is the high load ratio member failure mechanism. In this scenario, the column is unable to carry additional forces due to high temperatures, exceeding its maximum carrying capacity resulted in a failure.

Another mode of failure observed is cantilever beam mechanism. In this type of failure, upper half of beam thickness is in tension due to large displacement because of the collapse of column. The upper half tries to elongate fibers and the lower half on the other end compresses. This leads to the crushing of fibers and eventually collapse of beam. Failure of three members has resulted in the collapse of the whole structure without much warning.

Similar failure mode is observed in the case 5. However, as described by [37], another mode of failure has occurred which is pull-in force mechanism. In this failure, heating and buckling of an inner column result in the attached beams to act as catenary. In catenary action, the beams try to transfer the additional stresses away to the adjacent members. The load redistribution increases the compressive forces in the columns of same floor and the floors below. Lateral pull in force is developed in catenary action of beams. This also leads to the failure of structure. The side columns were loaded at 30% of their maximum load carrying capacity at ambient temperature. At collapse, an increase of 40% of forces was observed in both scenarios.

5.3.3 Deflections

To compare all the scenarios with each other, deformations are measured on the heated column. Vertical displacements are measured at the top node of the column and horizontal displacements are measured at the mid-length. The graphs obtained are shown below:

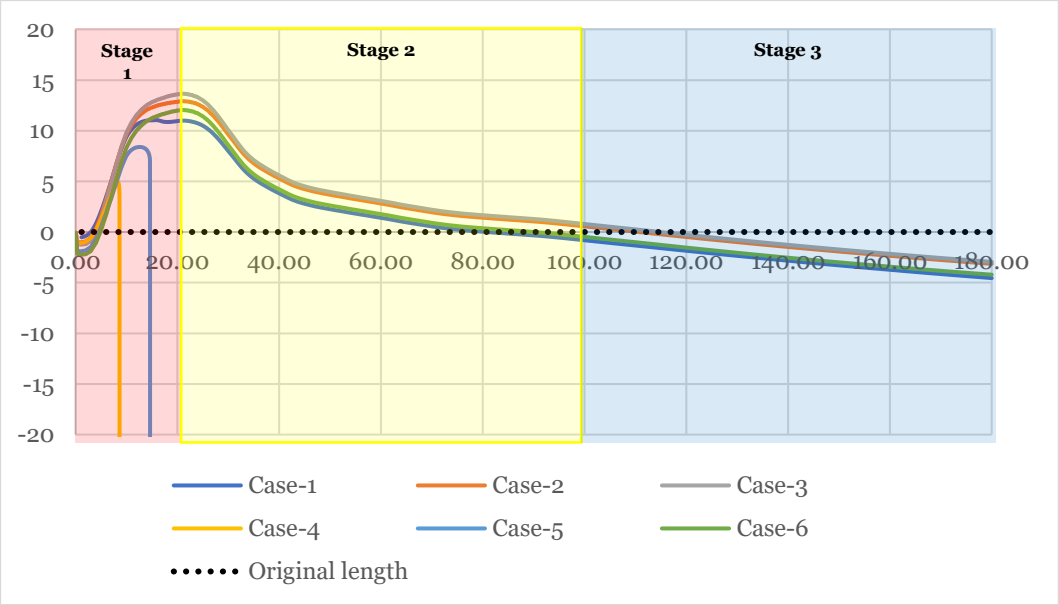

Figure 39 Vertical deflections at top node of heated column in each case scenario.

As can be seen from the graph, all columns expand at the heating phase and after cooling, shrink to the length shorter than their original length. The presence of restraints in the form of adjacent members and support conditions, reduce the maximum deflection of the columns. In this way, case-3 has recorded maximum deflection due to its location.

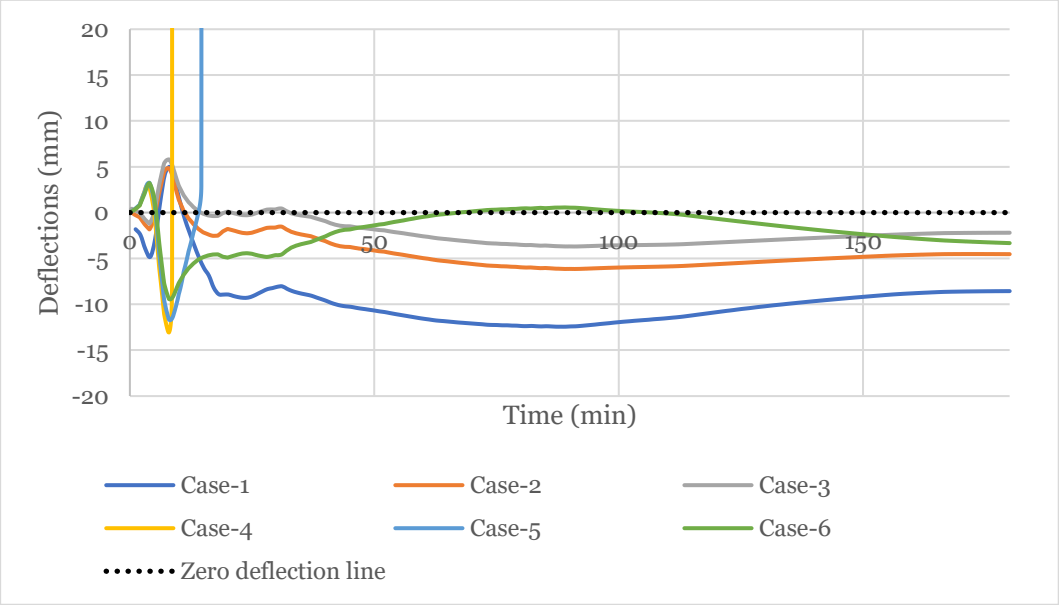

Figure 40 Horizontal deflections at centre of heated column in each case scenario.

The horizontal deflection at the center of columns indicates that presence of restrains in case-1 develop more stresses in the column and prohibit it to come back to its original shape even after the cooling phase. The failure of columns in case 4 and 5 can be seen in the graphs.

5.3.4 Further Investigation

Further investigation is done on the frame structure in two ways.

Addition of Bay

It is investigated that if the addition of one more bay to the frame will improve the forces redistribution mechanism or not. Addition of one bay brings one more axis of symmetry to the structure and it may improve the overall performance in forces redistribution. The bay is added to the right side of the frame and only two cases are investigated, namely as case-4 and 5, where the frame collapsed earlier.

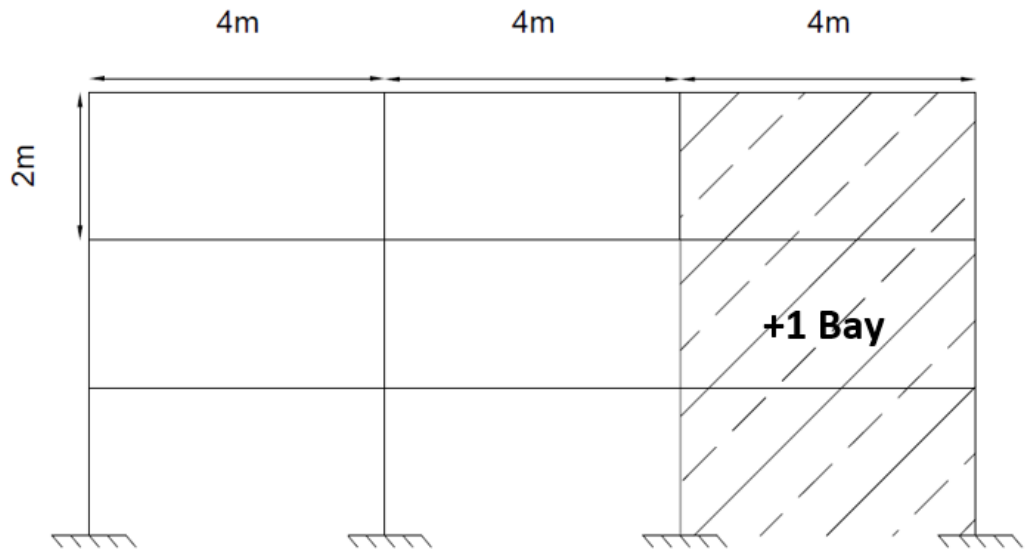

Figure 41 Addition of Bay to the frame for further investigation.

The forces redistribution occurred on the new frame however, it has been found that the frame collapses at time slightly later than the original frame. The collapse of frame in both case 4 and case 5 is shown below. The failure mechanism is same as described earlier for the original frame i.e. high load ratio member failure, cantilever beam and pull-in force failure mechanism.

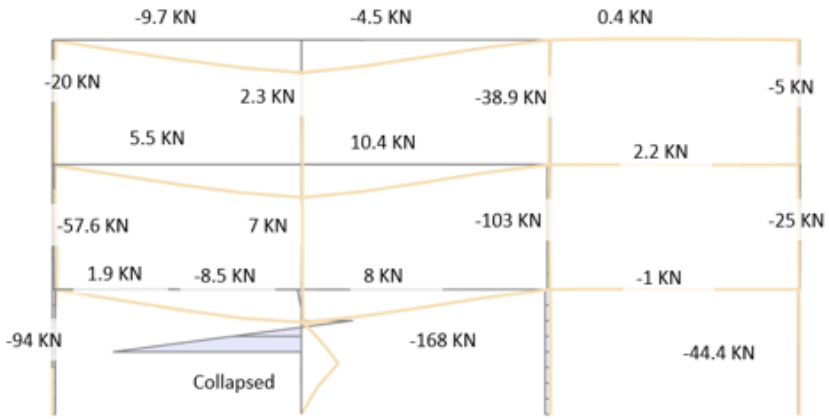

Case-4 @ 496 sec

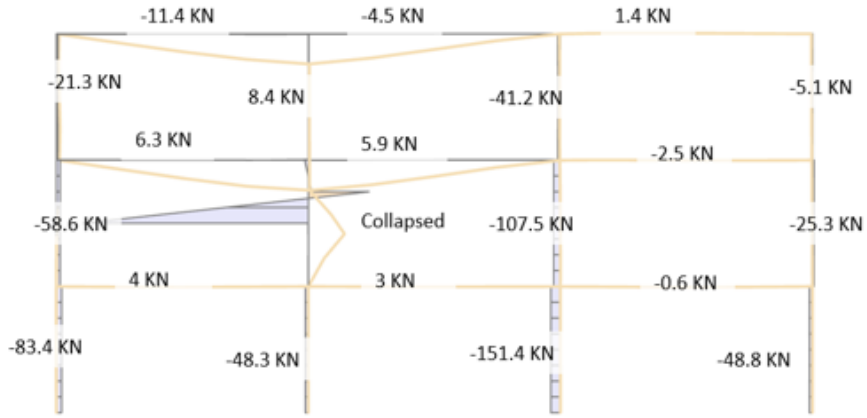

Case-5 @ 1001 sec

Figure 42: Forces redistribution at the collapse of frame with additional bay.

The vertical and horizontal deflections measured at the top node and mid-length of failed columns are mentioned in the graphs below.

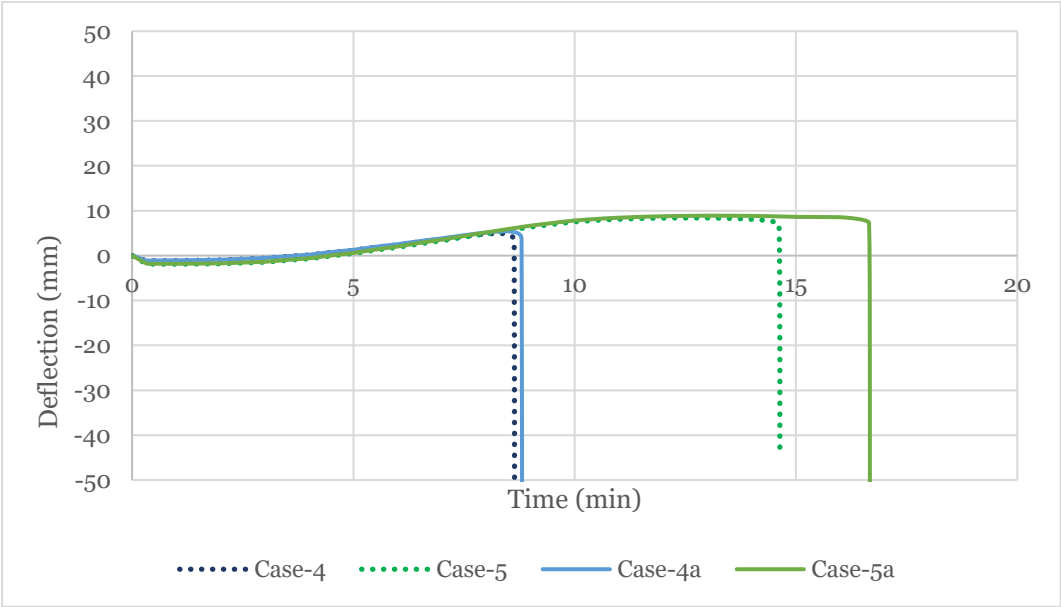

Figure 43: Comparison of vertical deflection with an additional bay to the frame.

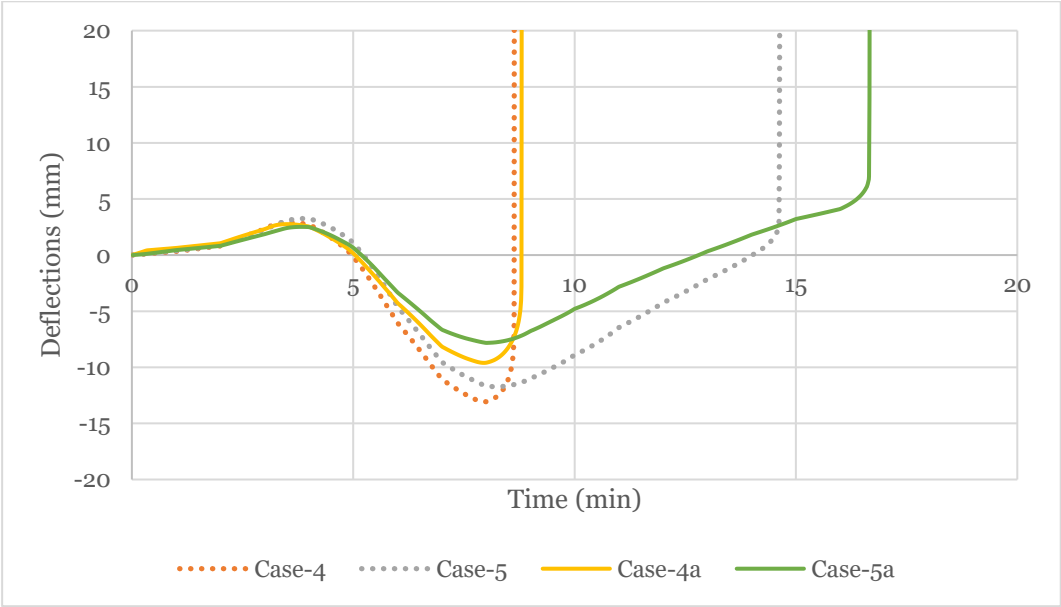

Figure 44 Comparison of horizontal deflections with an additional bay to the frame.

The graphs of horizontal and vertical deflections prove that the addition of one more bay does not improve the load distribution mechanism and therefore does not improve the time for structure to collapse. There is only improvement of 5 minutes with addition of bay for the structure to collapse in case 5 where the fire was on first floor.

Increased column stiffness

Further investigation is carried out to find the effect of increasing the stiffness of columns for critical scenarios where the frame was collapsing. This is also known as strong-column weak-beam theory where the stiffer column is better able to resist increased loads.

The middle columns of ground floor and first floor is replaced by a stiffer column section which has more capacity to resist fire induced loads. The geometrical properties of the section are as:

Table 7 Geometrical properties of new column with increased stiffness.

Section Properties	Column	Geometry
Type	Cold-formed square hollow section	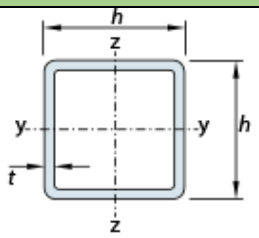
Depth (mm)	120	
Height (mm)	120	
Thickness (mm)	4	
Area of section (cm2)	18.1	
Mass/m	14.2	

The forces redistribution mechanism at the peak of heating and after cooling for both cases 4 and 5 are shown below:

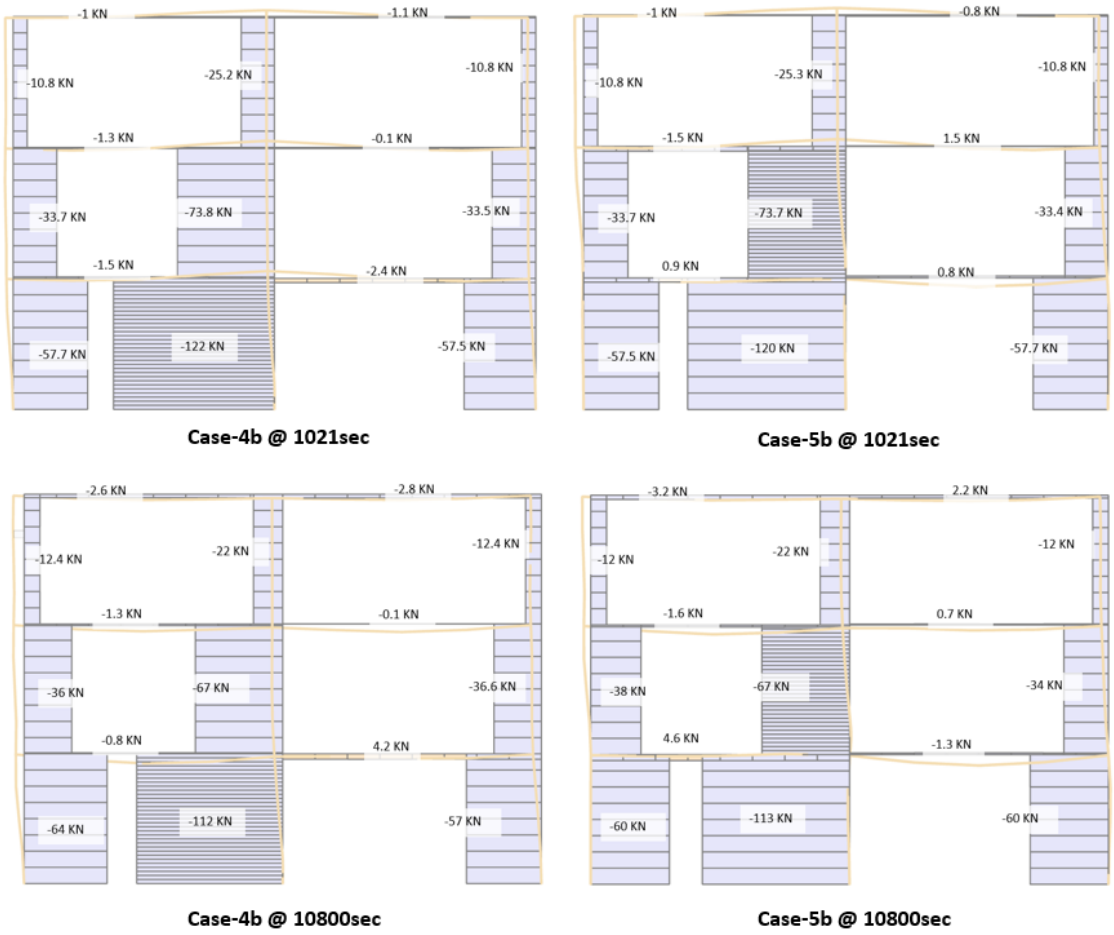

Figure 45 Forces redistribution in new frame with stiffer ground floor columns.

As can be seen that stiffer columns are better able to resist loads and redistribute to the adjacent structural elements. The higher load carrying capacity of the section at ambient temperatures is beneficial for the scenarios where localized fire affects one column. However, it has been found that stiffer sections shrink more after cooling and forces are higher in other members after the extinguishment of fire.

The horizontal and vertical deflections measured and comparison to the initial frame is presented below:

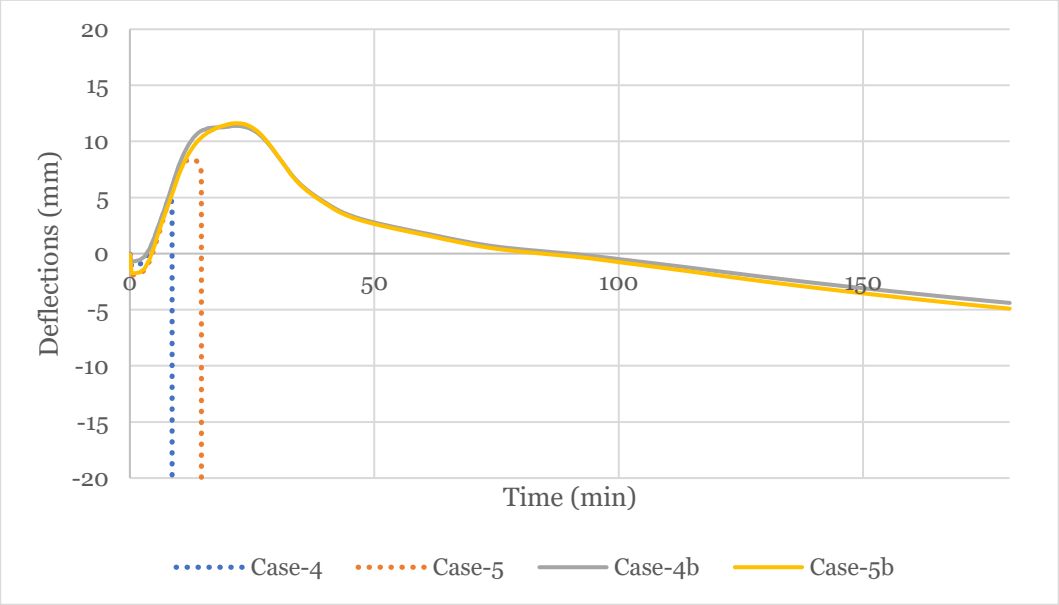

Figure 46: Vertical deflections at top node of stiffer heated columns compared with original frame.

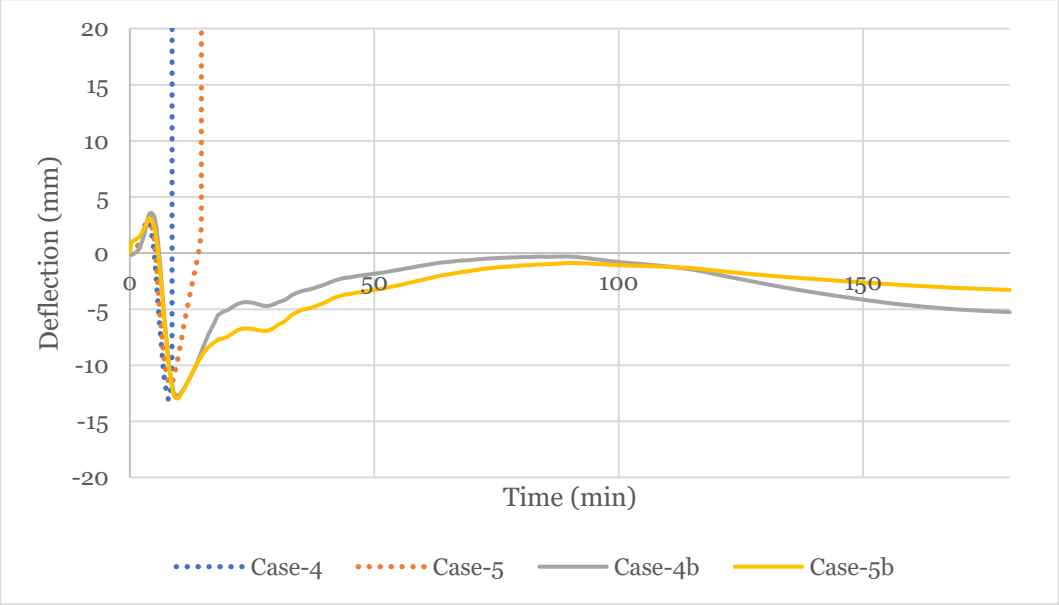

Figure 47: Horizontal deflections at mid-length of stiffer heated column compared with original frame.

As can be seen from the graph that the end restraint condition of fix support at the bottom of ground floor columns prevents it to comeback to its original position after the heating phase. As discussed earlier, this is due to the development of additional stresses. The shrinkage of column to length shorter than its original length results in continuos redistribution of forces even after the fire has stopped and the struture is cooled down.

6 Discussion

This research study demonstrates the coupling between FDS and SAFIR by importing boundary conditions using an adiabatic surface temperature device. The accuracy of results obtained using this approach is satisfactory as indicated by the validation study where the thermo-mechanical response of the steel column is in good agreement with the experimentally reported data. However, just like any other fire or structural analysis, several assumptions and uncertainties exist in this study which are discussed in detail.

The fire analysis was done based on the data found in literature. A prescribed heat release rate was chosen for burner and crib fire which resulted in reasonable results but not exactly the same as experimental data. Predicting the fire behaviour and flame development in CFD is challenging and depends on the mesh size however, due to limited time and computational resources available, a coarser mesh was chosen. The computational domain in CFD was also limited which may have an impact on the flow of hot gases and eventually the surface temperature of steel.

Thermal analysis in SAFIR was initially run in 3-D problem type however due to the inability of the software to calculate the heat transfer through a void in 3-d, the analysis was performed in 2-D. It was assumed that a temperature remains constant over a surface section and therefore output from one AST device was applied to one section of the geometry. This assumption is not very accurate as the temperature varies significantly over the height. Importing more AST files result in a complex situation where the problem gets more complicated as the transfer of boundary conditions is not automatic in SAFIR. A simple human error may result in a faulty output. In 2-D analysis, SAFIR calculates slightly lower temperature, and this is due to the negligence of conduction from bottom to top (Z-axis). This phenomenon of conduction in third dimension cannot be captured in 2-D thermal analysis. An additional constraint while working in SAFIR was the limited number of nodes for defining mesh. The current version of the GID-SAFIR interface available at BRE supports only 1010 nodes which is not enough for creating a fine mesh. Due to this limitation, all analysis were done on a coarse mesh. Similarly, structural analysis was done by assigning four 2-D thermal output files to a column. It was assumed that the behaviour of these 4 sections will display the response of the whole column. Again, this assumption is overly conservative since the time-temperature data is varying significantly over the height. A sensitivity analysis is done by assigning 15 thermal output files to a structural model however, no conclusion could be drawn on the fact that assigning more AST files always results in accurate structural response.

In the case study of the progressive collapse mechanism, the loads were assumed for the frame in such a way that the central ground floor column is at 65% of its maximum load carrying capacity at ambient temperatures. The

side columns of the frame are loaded at 30% of their maximum capacity. These loading conditions are different in every structure and have an impact on the overall performance when exposed to fire. Furthermore, it is assumed that only one column is subjected to fire in each scenario and the rest of the structure remains under ambient conditions. This assumption is not realistic as the fire in a storey or compartment affects other structural members and has an influence on the behaviour of the frame. The SAFIR calculations could not calculate further where substantial displacements were measured. It is assumed that the whole structure collapses where a significant part fails however, this may not always be true. The connections between columns and beams are considered as a fix however, in a practical scenario, some of the connections may be pin or semi-rigid, such configuration may present a completely different phenomena of forces redistribution between members.

7 Conclusion

In this study, the results from the one-way coupling between a CFD and FE package are presented. A built-in tool of adiabatic surface temperature in FDS is utilized for transferring boundary conditions into SAFIR, an FE software.

The coupling method is validated using experimental data where a steel column is exposed to a localized fire. Thermo-mechanical response using the FE package is compared with the experimental data. The results from FDS-SAFIR coupling are in good agreement with the experimental data however some discrepancies are noted at various time intervals. It is found that the 3-D thermal analysis in SAFIR is unable to calculate the heat transfer through the void and the results are not accurate. Defining an internal cavity is important as the dominant modes of heat transfer are radiation and convection through voids. A 2-D thermal analysis including the heat transfer through void calculated accurate temperature on the front face and corner, however, there is still some difference on the side and back face. A sensitivity analysis indicated that the emissivity of steel assumed, and the convective heating and cooling coefficients influence the temperature development. Similarly, the mechanical response is compared in terms of horizontal and vertical displacements. The mechanical response is in good agreement however at several time intervals, there are differences. SAFIR underestimates the peak horizontal deflection in the heating phase and then overestimates with a constant value until the fire is extinguished. In the cooling phase, SAFIR underestimates the horizontal and vertical deformations. A sensitivity analysis has found that importing a greater number of AST files from CFD simulation does not always improve accuracy.

The AST-gas device in FDS calculates a lower temperature than the AST-surface device. It is found that the geometry of the steel section impacts fire and temperature development in the simulation. As reported earlier in the literature section, a member closer to the fire source should be modelled in the CFD package to capture the real temperature development. Importing output from AST-gas device seriously underestimates the thermal response of steel and therefore, has not been used for subsequent mechanical analysis.

The validation methodology is then used to study the forces redistribution and a progressive collapse mechanism in a planar frame when subjected to a localized fire. It is noted that the additional fire-induced stresses are redistributed to adjacent members of the structure. Sometimes it leads to loading and sometimes to unloading of adjacent members eventually improving the overall performance. During a cooling phase, loss of material properties results in the shortening of the column, and it contracts to a length shorter than its original length. This causes the redistribution of forces again in the cooling phase. It indicates that a cooling phase is also critical for the overall

performance of a structure and should be considered in the design phase. A comparison of different fire locations has highlighted that the central ground floor column and first-floor column are more vulnerable to fire-induced progressive collapse. The analysis shows that a variety of phenomena like high load ratio, cantilever beam and pull-in force mechanism are responsible for such collapse. Further investigation has highlighted that the addition of one bay to the frame does not significantly improve the forces redistribution however, increasing the stiffness of ground floor columns, a strong column weak beam configuration, does improve the overall stability and performance.

The results from this study indicate that one-way coupling between CFD and FE can predict an accurate thermo-mechanical response however the accuracy depends on several factors. These factors are not easy to address as each fire scenario is different and comes with its own variables. This study also shows that the computation and analysis time can be saved by performing one fire analysis and obtaining various mechanical responses based on the location of the fire. Poor performance of ground floor columns indicates that it is important to limit the fire to the critical members of the structure.

8 References

[1] C. Zhang and G. Q. Li, "Fire dynamic simulation on thermal actions in localized fires in large enclosure," *Adv. Steel Constr.*, vol. 8, no. 2, pp. 124–136, 2012.

[2] G. M. Faeth, *An introduction to fire dynamics*, vol. 66, no. 1. 1986.

[3] E. Commission, D.-G. for R. and Innovation, L. Twilt, D. Martin, B. Kirby, and M. O'Connor, *Behaviour of multi-storey, steel framed building subjected to natural fire effects : final report*. Publications Office, 2002.

[4] K. Prasad and H. R. Baum, "Coupled fire dynamics and thermal response of complex building structures," *Proc. Combust. Inst.*, vol. 30, no. 2, pp. 2255–2262, 2005, doi: 10.1016/j.proci.2004.08.118.

[5] C. Couto and P. Vila Real, "The influence of imperfections in the critical temperature of I-section steel members," *J. Constr. Steel Res.*, vol. 179, p. 106540, 2021, doi: 10.1016/j.jcsr.2021.106540.

[6] C. Arya, "Eurocode 3: Design of steel structures," *Des. Struct. Elem.*, vol. 3, no. 1, pp. 395–453, 2015, doi: 10.1201/b18121-19.

[7] T. Gernay and A. Gamba, "Behaviour of Steel Frame Structures Under Localised Fire Including Progressive Collapse During Cooling," *Struct. Fire*, no. February 2020, 2018.

[8] M. Malendowski and A. Glema, "Development and Implementation of Coupling Method for CFD-FEM Analyses of Steel Structures in Natural Fire," *Procedia Eng.*, vol. 172, pp. 692–700, 2017, doi: 10.1016/j.proeng.2017.02.082.

[9] H. R. Baum, "Simulating fire effects on complex building structures," *Fire Saf. Sci.*, pp. 3–18, 2005, doi: 10.3801/IAFSS.FSS.8-3.

[10] N. Tondini, O. Vassart, and J. Franssen, "Development of an Interface Between Cfd and Fe Software," *7th Int. Conf. Struct. Fire*, no. December 2015, pp. 459–468, 2012.

[11] S. Welch, S. Miles, S. Kumar, T. Lemaire, and A. Chan, "FIRESTRUC - Integrating advanced three-dimensional modelling methodologies for predicting thermo-mechanical behaviour of steel and composite structures subjected to natural fires," *Fire Saf. Sci.*, pp. 1315–1326, 2008, doi: 10.3801/IAFSS.FSS.9-1315.

[12] J. L. Torero, A. Law, and C. Maluk, "Defining the thermal boundary condition for protective structures in fire," *Eng. Struct.*, vol. 149, pp. 104–112, 2017, doi: 10.1016/j.engstruct.2016.11.015.

[13] J. C. G. Silva, A. Landesmann, and F. L. B. Ribeiro, "Interface model to fire-thermomechanical performance-based analysis of structures under fire conditions," *Fire Evacuation Model. Tech. Conf. 2014*, no. December 2015, 2014.

[14] U. Wickstr, "Calculating Heat Transfer To Fire Introduction," no. January, 2015.

[15] F. Pesavento, M. Pachera, B. A. Schrefler, D. Gawin, and A. Witek, "Coupled numerical simulation of fire in tunnel," *AIP Conf. Proc.*, vol. 1922, no. January, 2018, doi: 10.1063/1.5019085.

[16] D. Banerjee, W. Hess, T. Olano, J. Terrill, and J. Gross, "Visualization of structural behavior under fire," *U.S. Dep. Commer.*, no. August, pp. 1–28, 2009, [Online]. Available: http://math.nist.gov/mcsd/savg/papers/VisualizationFire-2009.pdf.

[17] F. Pesavento, B. A. Schrefler, D. Gawin, and J. Principe, "Fully coupled numerical simulation of fire in tunnels: From fire scenario to structural response," *MATEC Web Conf.*, vol. 6, 2013, doi: 10.1051/matecconf/20130605005.

[18] A. A. Khan, A. Usmani, and J. L. Torero, "Evolution of fire models for estimating structural fire-resistance," *Fire Saf. J.*, vol. 124, no. April, 2021, doi: 10.1016/j.firesaf.2021.103367.

[19] X. Yan and T. Gernay, "Numerical modeling of localized fire exposures on structures using

FDS-FEM and simple models," *Eng. Struct.*, vol. 246, no. April, p. 112997, 2021, doi: 10.1016/j.engstruct.2021.112997.

[20] J. C. G. Silva, A. Landesmann, and F. L. B. Ribeiro, "Fire-thermomechanical interface model for performance-based analysis of structures exposed to fire," *Fire Saf. J.*, vol. 83, pp. 66–78, 2016, doi: 10.1016/j.firesaf.2016.04.007.

[21] J. M. Franssen and T. Gernay, "Modeling structures in fire with SAFIR®: Theoretical background and capabilities," *J. Struct. Fire Eng.*, vol. 8, no. 3, pp. 300–323, 2017, doi: 10.1108/JSFE-07-2016-0010.

[22] X. Yan and T. Gernay, "Numerical modeling of localized fire exposures on structures using FDS-FEM and simple models," *Eng. Struct.*, vol. 246, no. April, 2021, doi: 10.1016/j.engstruct.2021.112997.

[23] D. Duthinh, K. McGrattan, and A. Khaskia, "Recent advances in fire-structure analysis," *Fire Saf. J.*, vol. 43, no. 2, pp. 161–167, 2008, doi: 10.1016/j.firesaf.2007.06.006.

[24] S. N. Wickstrom Ulf, D. Duthinh, and K. Mcgrattan, "Adiabatic Surface Temperature for Calculating Heat Transfer To Fire Introduction," *Most*, vol. 2, 2007, [Online]. Available: https://www.nist.gov/publications/adiabatic-surface-temperature-calculating-heat-transfer-fire-exposed-structures.

[25] A. Byström, U. Wickström, and M. Veljkovic, "Use of Plate Thermometers for Better Estimate of Fire Development," *Appl. Mech. Mater.*, vol. 82, pp. 362–367, 2011, doi: 10.4028/www.scientific.net/AMM.82.362.

[26] J. Sandström, *Thermal boundary conditions based on field modelling of fires. Heat transfer calculations in CFD and FE models with special regards to fire exposure renresented with adiabatic surface temperature. Licentiate thesis.* 2013.

[27] G. Q. Li and C. Zhang, "Integrated fire-structure simulation of a localzied fire test on a ceiling steel beam," *Adv. Steel Constr.*, vol. 13, no. 2, pp. 132–143, 2017, doi: 10.18057/IJASC.2017.13.2.3.

[28] K. McGrattan, S. Hostikka, R. McDermott, J. Floyd, C. Weinschenk, and K. Overhold, "Sixth Edition Fire Dynamics Simulator User 's Guide (FDS)," *NIST Spec. Publ. 1019*, vol. Sixth Edit, 2020.

[29] K. McGrattan, S. Hostikka, R. McDermott, J. Floyd, C. Weinschenk, and K. Overholt, "Sixth Edition Fire Dynamics Simulator Technical Reference Guide Volume 1 : Verification guide," vol. 1, pp. 1–147, 2015.

[30] J. Sandström, *Thermal Boundary Conditions Based on Field Modelling of Fires*. 2013.

[31] O. Vassart *et al.*, "3D simulation of Industrial Hall in case of fire. Benchmark between ABAQUS, ANSYS and SAFIR," *10th Int. Fire Sci. Eng. Conf.*, no. October 2014, 2004.

[32] N. Tondini, A. Morbioli, O. Vassart, S. Lechêne, and J. M. Franssen, "An integrated modelling strategy between a CFD and an FE software: Methodology and application to compartment fres," *J. Struct. Fire Eng.*, vol. 7, no. 3, pp. 217–233, 2016, doi: 10.1108/JSFE-09-2016-015.

[33] J. Ferreira, J.-M. Franssen, T. Gernay, and A. Gamba, "Validation of SAFIR ® through DIN EN 1992-1-2 NA Comparison of the results for the examples presented in Annex CC," vol. 32, no. 0, pp. 1–70, 2018.

[34] J. Ferreira, T. Gernay, J. Franssen, and O. Vassant, "Discussion on a systematic approach to validation of software for structures in fire - Romeiro Ferreira Joao Daniel," *SiF 2018 10th Int. Conf. Struct. fire*, 2018.

[35] R. Zaharia and T. Gernay, "Validation of the Advanced Calculation Model SAFIR through DIN EN 1991-1-2 Procedure," pp. 841–848, 2012, doi: 10.3850/978-981-07-2615-7_291.

[36] "SAFIR Technical documentation Description of SAFIR A . 1 Purpose of SAFIR," vol. 2008, pp. 1–14, 2011.

[37] B. Jiang, G. Q. Li, and A. Usmani, “Progressive collapse mechanisms investigation of planar steel moment frames under localized fire,” *J. Constr. Steel Res.*, vol. 115, pp. 160–168, 2015, doi: 10.1016/j.jcsr.2015.08.015.

[38] E. Rackauskaite and J. El-Rimawi, “A Study on the Effect of Compartment Fires on the Behaviour of Multi-Storey Steel Framed Structures,” *Fire Technol.*, vol. 51, no. 4, pp. 867–886, 2015, doi: 10.1007/s10694-014-0419-0.

[39] R. Sun, I. Burgess, and Z. Huang, “Behaviour of frame columns in localised fires,” *J. Struct. Fire Eng.*, vol. 4, no. 3, pp. 175–186, 2013, doi: 10.1260/2040-2317.4.3.175.

[40] J. Y. R. Liew, L. K. Tang, T. Holmaas, and Y. S. Choo, “Advanced analysis for the assessment of steel frames in fire,” *J. Constr. Steel Res.*, vol. 47, no. 1–2, pp. 19–45, 1998, doi: 10.1016/S0143-974X(98)80004-7.

[41] P. Covi, G. Abbiati, N. Tondini, O. S. Bursi, and B. Stojadinovic, “A static solver for hybrid fire simulation based on model reduction and dynamic relaxation,” pp. 556–566, 2020, doi: 10.14264/2ed186c.

[42] C. Zhang, J. G. Silva, C. Weinschenk, D. Kamikawa, and Y. Hasemi, “Simulation Methodology for Coupled Fire-Structure Analysis: Modeling Localized Fire Tests on a Steel Column,” *Fire Technol.*, vol. 52, no. 1, pp. 239–262, 2016, doi: 10.1007/s10694-015-0495-9.

[43] Kamikawa D, Y. Hasemi, K. Yamada, and M. Nakamura, “Mechanical response of a steel column exposed to a localized fire.,” *Proc. fourth Int. Work. stuctures fire, Aveiro, Port.*, p. pp 225–234, 2006.

[44] “User Manual,” *SpringerReference*, 2011, doi: 10.1007/springerreference_28001.

[45] J. Franssen and T. Gernay, “Diamond 2016,” vol. 2016, 2016.

[46] T. Gernay and J. M. Franssen, “Johns Hopkins University , Baltimore Example : steel beam with 3D solid elements ‘ Loaded steel beam heated from below , modeled with solid FE ,’” pp. 1–17, 2019.

[47] J.-M. Franssen and T. Gernay, “Users’ Manual for SAFIR 2019 - Thermal Analysis,” no. January, 2019.

[48] A. C. Program, F. O. R. Analysis, O. F. Structures, and S. T. O. Fire, “Safir 2019,” no. February, 2020.

[49] K. A. M. Moinuddin, J. S. Al-Menhali, K. Prasannan, and I. R. Thomas, “Rise in structural steel temperatures during ISO 9705 room fires,” *Fire Saf. J.*, vol. 46, no. 8, pp. 480–496, 2011, doi: 10.1016/j.firesaf.2011.08.001.

[50] British Standards Istitute, “No Title,” 2020. [Online]. Available: https://www.thenbs.com/PublicationIndex/documents/details?Pub=BSI&DocID=328626.

Appendix A: Steel material properties for SAFIR analysis

The steel material chosen for analysis in SAFIR was taken as Carbon steel which is by default incorporated in the SAFIR material as 'STEELEC3EN'. The temperature dependent material properties are taken from EN 1993-1-2 and are presented in the form of graphs below.

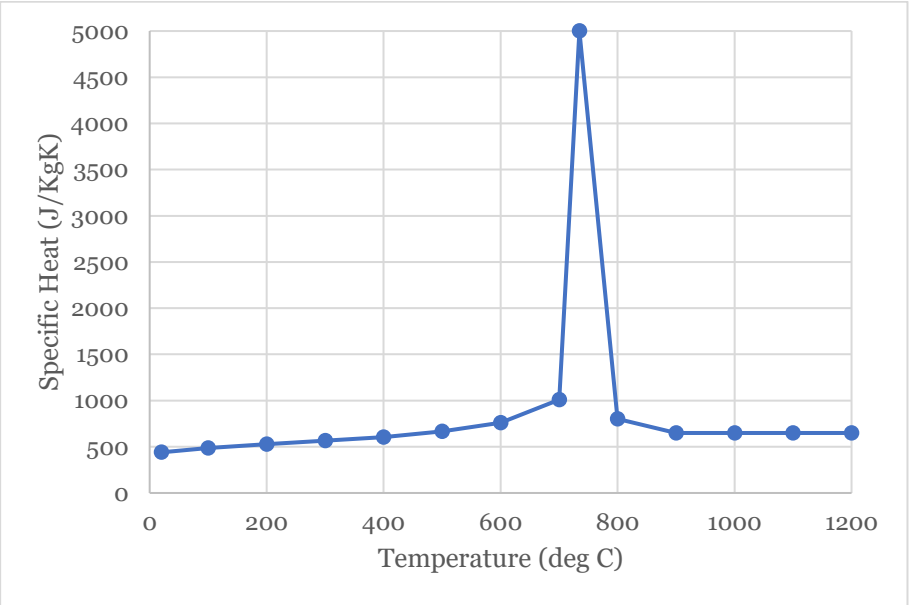

Figure 48: Specific heat of carbon steel as a function of temperature

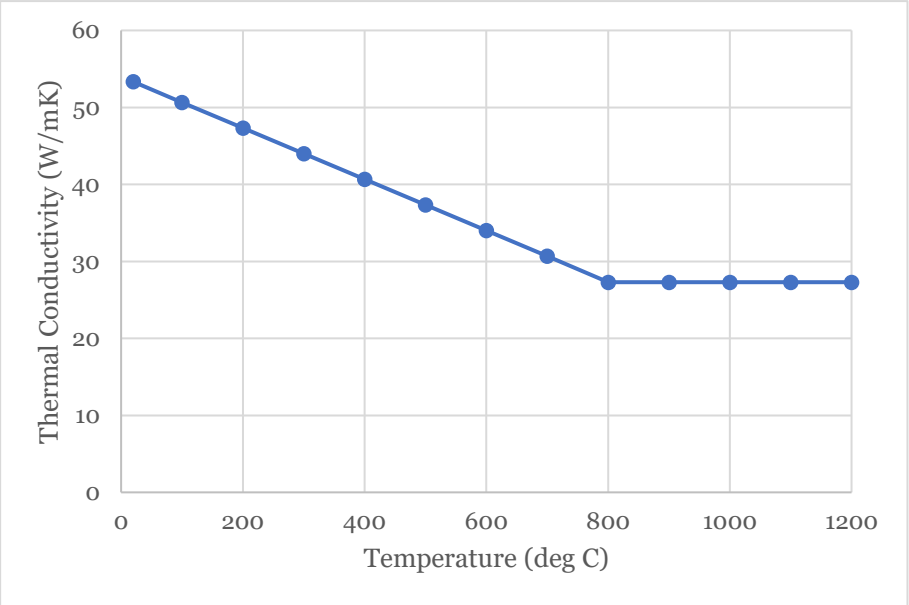

Figure 49: Thermal conductivity of carbon steel as a function of temperature

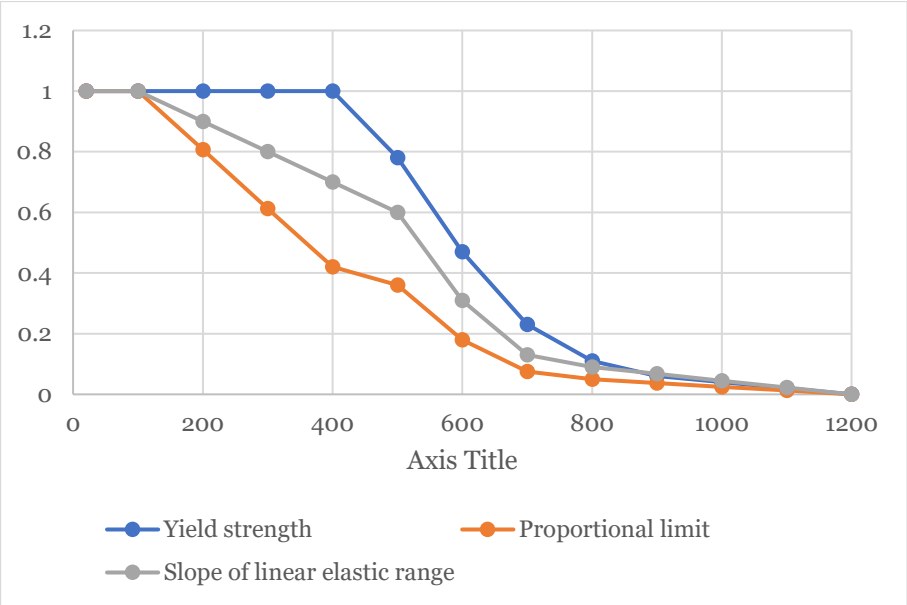

Figure 50: Reduction factors for stress-strain relationship of carbon steel at elevated temperatures

Appendix B: Comparison of experimental results and thermal response validation

The difference of temperatures obtained with 2-D thermal analysis using SAFIR and reported by experimental data is illustrated in the form of tabulated data and graphs below:

Table 8 Average % difference in temperatures measured at front face at various heights.

Time Interval	Front Surface			
(min)	400mm	600mm	800mm	1200mm
0-10	13.53	3.23	14.13	14.14
10-60	8.03	3.84	4.45	9.08
60-120	25.85	18.82	7.56	31.57

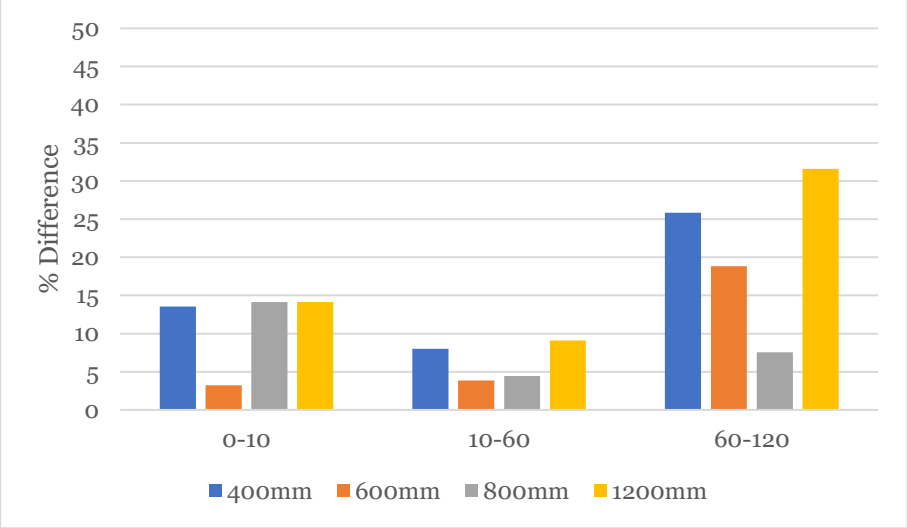

Figure 51 The % difference in the temperature obtained by SAFIR and reported by experimental data at front face.

Table 9 Average % difference in temperatures measured on corner at various heights.

Time Interval	Corner		
(min)	400mm	800mm	1200mm
0-10	12.63	12.45	14.36
10-60	13.14	4.54	15.1
60-120	23.78	6.59	29.87

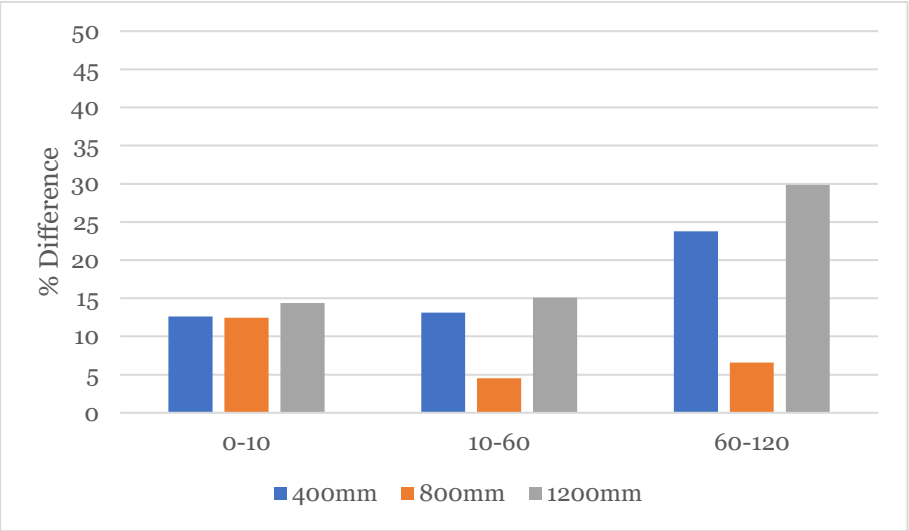

Figure 52 The % difference in the temperature obtained by SAFIR and reported by experimental data at corner.

Table 10 Average % difference in temperatures measured on the right face at various heights.

Time Interval	Side (right)		
(min)	400mm	600mm	1200mm
0-10	12.03	6.93	11.93
10-60	18.18	4.51	19.73
60-120	23.9	15.85	27.63

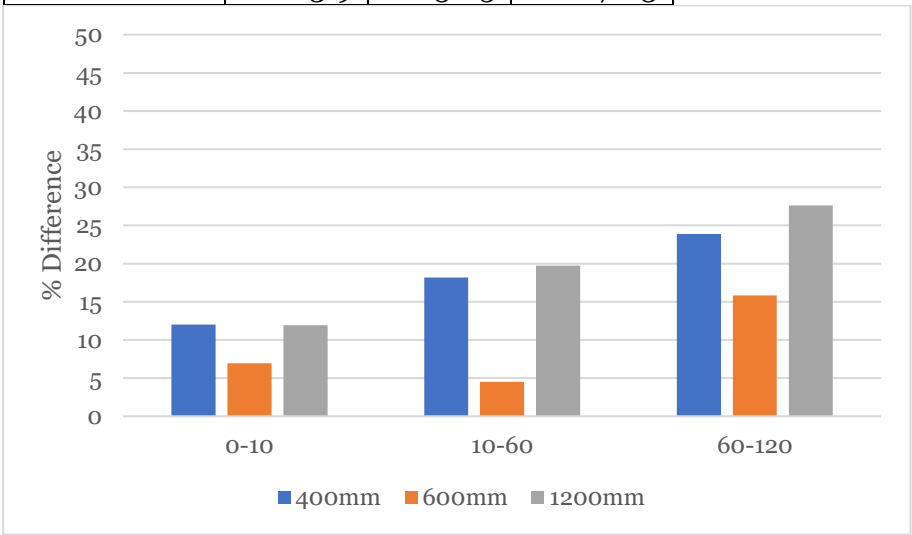

Figure 53 The % difference in the temperature obtained by SAFIR and reported by experimental data at right side surface.

Table 11 Average % difference in temperatures measured on the left side at various heights.

Time Interval	Side (Left)	
(min)	400mm	600mm
0-10	16.62	10.6
10-60	26.39	13.61
60-120	25.99	17.11

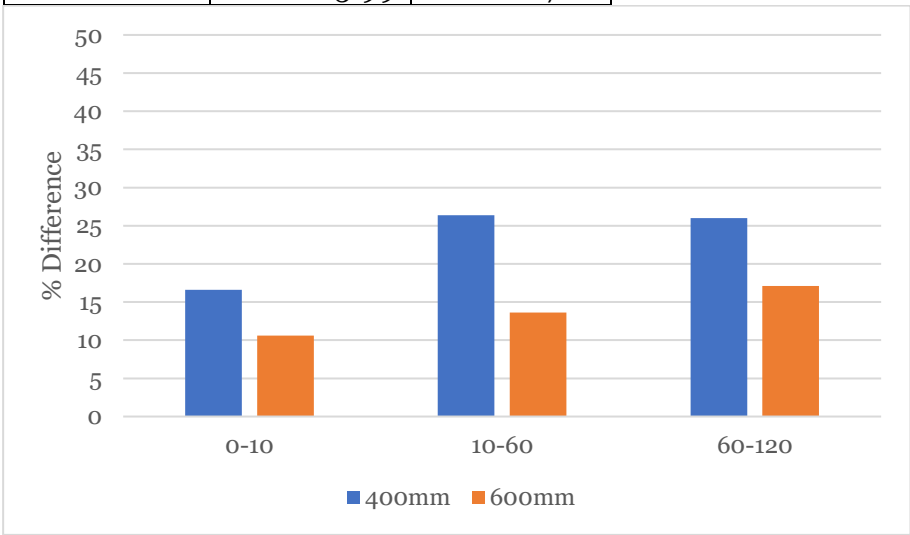

Figure 54 The % difference in the temperature obtained by SAFIR and reported by experimental data at left side surface.

Table 12 Average % difference in temperatures measured on the back face at various heights.

Time Interval	Back Surface		
(min)	400mm	600mm	1200mm
0-10	18.6	12.6	9.34
10-60	32.68	13.61	24.77
60-120	26.34	18.3	24.74

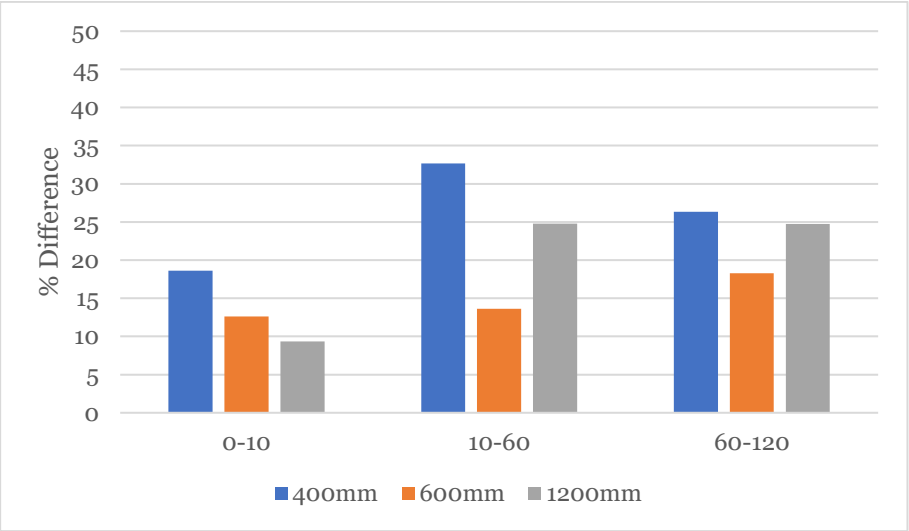

Figure 55 The % difference in the temperature obtained by SAFIR and reported by experimental data at back side surface